

1 **Design and Characterization of LDH-Modified Biochar as a Nanoadsorbent for Copper**
2 **Removal: A Response Surface Methodology Approach**

3 **M. Shafiq^{a,*}, M. T. Amin^b, A. A. Alazba^{a,c}**

4 ^a Water Research Chair, King Saud University, Riyadh 11451, Saudi Arabia.

5 ^b Civil and Environmental Engineering Department, College of Engineering, King Faisal
6 University, Al-Ahsa 31982, Saudi Arabia

7 ^c Department of Agricultural Engineering, College of Food and Agricultural Sciences, King Saud
8 University, Riyadh 11451, Saudi Arabia.

9

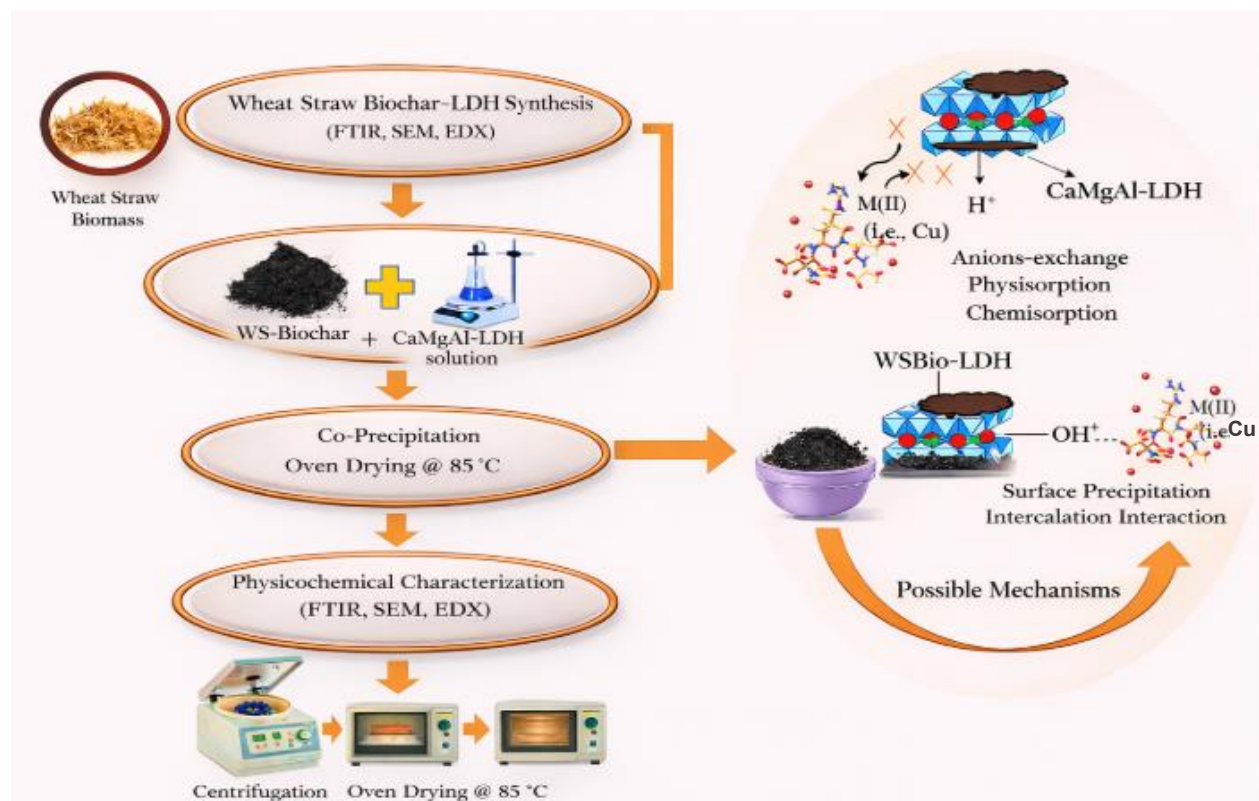
10 ** Corresponding Author: M. Shafiq, E-mail: mshrana@ksu.edu.sa*

11 **Abstract**

12 This study reports the layered double hydroxides' modified wheat straw biochar (WsBio-LDH
13 composite) composite as an effective adsorbent for the removal of copper ions (Cu^{2+}) from
14 aqueous solution. The WsBio-LDH composite adsorbent was analyzed using central composite
15 design and response surface methodology (RSM). RSM optimized parameters for Cu^{2+} removal
16 using the WsBio-LDH composite were found to be 87.06 min for the contact time, 0.491 g for
17 the adsorbent dose, 5.93 for the solution pH, and 12.75 mg/L for the initial Cu^{2+} concentration. A
18 significant correlation between predicted and experimental values was observed with 99 %
19 removal exhibiting a deviation of less than 1% that validates the model's accuracy. All individual
20 batch variables significantly ($p < 0.0001$) influenced the Cu^{2+} removal efficiency using the
21 WsBio-LDH composite. Both the contact time and initial Cu^{2+} concentrations displayed negative
22 effects while the solution pH and Cu^{2+} concentrations exerted a positive interactive effect (p
23 < 0.0049) on Cu^{2+} removal efficiency using the WsBio-LDH composite. The Langmuir model
24 accurately represented a monolayer adsorption of Cu^{2+} onto the surface of the WsBio-LDH
25 composite. The pseudo-second order kinetic model provided the best fit for the adsorption
26 kinetics of the WsBio-LDH composite. FTIR spectra revealed various functional groups on the
27 surface of the WsBio-LDH composite before and after Cu^{2+} adsorption. The SEM images
28 indicated a rough surface with two distinct phases of raw biochar and micro-sized Ca/Al/Mg-
29 LDH particles, and roughness enhances further after the Cu^{2+} adsorption. EDX analysis further

30 confirms the adsorption of Cu^{2+} . These results underscore the efficacy of the WsBio-LDH
31 composite as a promising nano-adsorbent for wastewater treatment applications.

32 **Keywords:** Copper removal, Monolayer adsorption, RSM optimization, WsBio-LDH composite



33

34

Graphical Representation of Removal of Cu^{+2}

35 Introduction

36 The need for clean water for everyday use is rising because of the fast expansion of the
37 population, commercialization, and civilization. Global concerns regarding heavy metal pollution
38 have gained significant attention in recent years due to their toxicity and bioaccumulation
39 potential. Industrial effluents and the discharge of untreated sanitary waste are ranked as the
40 primary sources that contribute to heavy metals pollution of aquatic environment (Bej et al.
41 2023). Heavy metals are non-biodegradable and hence persistent in aquatic environments
42 (Biswal and Balasubramanian 2023). Among heavy metals, copper (Cu^{2+}) is the most harmful
43 pollutant, which usually enters water systems through various industrial processes such as
44 mining, battery manufacturing, and paint production. Cu^{2+} contamination induces extreme health
45 risks, such as neurological damage and developmental disorders (Gaetke et al. 2014). It also

46 causes gastrointestinal distress with short-term exposure, while liver or kidney damage may
47 occur with long-term exposure. Therefore, it is direly needed to treat Cu^{2+} loaded effluents prior
48 to disposal freshwater environment. Many treatment strategies, including membrane filtration
49 (Mokhtar et al. 2018), ion exchange resin (Zakaria et al. 2023), coagulation (Luo et al. 2018) and
50 flocculation (Sun et al. 2022) have been applied to remove Cu^{2+} from waste streams. Various
51 technologies, including membrane-based extraction processes, have been investigated for the
52 removal of heavy metals from aqueous solutions (Fouad et al. 2017). However, membrane fouling
53 (Al-Rashdi et al. 2013), high working costs of ion exchange resins (Hagag et al. 2017), Cu^{2+} rich
54 sludge generation and secondary pollution (Kouniba et al. 2024), Cu^{2+} recover from sludge
55 (Trinh et al. 2021) and undesired retention of ions in ultrafiltration (Gräf et al. 2023) are
56 recognized drawbacks of these techniques. Advanced functional materials have also been
57 investigated for wastewater treatment applications. Recent studies reported that
58 nonstoichiometric Mn–Co spinel oxides effectively activate oxidants for the removal of organic
59 pollutants in continuous-flow wastewater treatment systems, demonstrating the importance of
60 engineered materials for environmental remediation (Liang et al.2026). Recent studies have also
61 demonstrated the effectiveness of advanced engineered materials for wastewater remediation.
62 For example, visible-light-activated $\text{CuFe}_2\text{O}_4/\text{Zn-BTC}$ photocatalysts have shown efficient
63 mineralization and detoxification of hazardous contaminants in industrial effluents, highlighting
64 the growing importance of multifunctional materials for environmental treatment applications
65 (Mahmood et al. 2026) Resource recovery and contaminant removal have become important
66 objectives in modern wastewater treatment systems. Recent investigations have demonstrated
67 simultaneous pollutant degradation and nutrient recovery using advanced oxidation processes,
68 emphasizing the growing need for sustainable remediation technologies (Wang et.al.2026). On
69 the other hand, adsorption presents as the best alternative due to its low cost, ease of application,
70 efficiency even at low concentrations, and environmentally friendly technique (Akhtar et al.
71 2025). Adsorption is an efficient process because it can remove several pollutants, including
72 biological and inorganic substances, which contain soluble and non-soluble compounds from
73 wastewater without producing toxic substances (Rashid et al. 2021). Various adsorbents such as
74 metal oxides (Liu and Wang 2013a), metal organic framework (Han et al. 2024), steel slag
75 (Mingming et al. 2023), Modified adsorbent hydroxypropyl cellulose xanthate (Zhang et al.
76 2016), and synthetic abalone shell hydroxyapatite microspheres (Wang et al. 2022) have been

77 explored in the literature for Cu^{2+} removal. However, naturally occurring adsorbents derived
78 from bio-resources offer significant advantages, including abundance, low cost, and
79 environmental sustainability (Dehghani et al. 2023).

80 Recent advances have demonstrated the role of intelligent and hybrid modeling approaches in
81 environmental remediation. For example, Internet of Things (IoT) enabled Recurrent Neural
82 Network (RNN) and Graph Neural Networks (GNN) based systems have been applied for real-
83 time wastewater monitoring and agricultural sustainability (Alprol et al. 2024; Tabassam et al.
84 2025). The development of economical and sustainable water reclamation systems has further
85 emphasized the need for efficient treatment materials capable of removing contaminants at low
86 operational cost (Syed et al, 2024). Although these studies focus on sensor-based intelligence,
87 material level innovations such as the WsBio-LDH composite remain essential for effective
88 pollutant removal, highlighting the complementary role of advanced adsorbents in smart water
89 treatment frameworks (Das et al. 2025).

90 Recent progress in sustainable environmental technologies has also emphasized the importance of
91 understanding material-level reaction mechanisms and surface interactions. For instance, mechanistic
92 studies on CO_2 conversion systems have demonstrated that catalyst surface properties and interfacial
93 reactions play a crucial role in determining pollutant transformation efficiency and process performance
94 (Hussain et al. 2026). Although the present work focuses on Cu^{2+} adsorption rather than catalytic CO_2
95 conversion, both fields highlight the significance of rational material design and surface engineering for
96 improving environmental remediation technologies.

97 In recent years, globally agriculture has produced millions of tons of agricultural bioresources,
98 including wheat straw (WS), which is ranked as the second largest lignocellulosic material
99 (Riseh et al. 2024). Every year, crop wastes are burned in fields, releasing a variety of pollutants
100 in the environment, like CO , particulate matter, and unburned hydrocarbons, and it is a common
101 practice worldwide. Consequently, environmental pollution increases, and valuable bioresources
102 are wasted. Therefore, it is imperative to transform agricultural waste into wealth through value
103 addition (Priya et al. 2025) and, importantly, to reduce pollution.

104 The growing emphasis on sustainable material development has encouraged the adoption of
105 green processing technologies and environmentally benign modification strategies across various
106 industrial sectors. Recent advances in deep eutectic solvent-based material modification have

107 demonstrated the potential of green chemistry approaches for enhancing material functionality
108 while minimizing environmental impacts (Farooq et al. 2025). Such developments further
109 support the need for sustainable adsorbent design for wastewater remediation.

110 The sustainable utilization of biomass and agricultural residues has gained increasing attention as
111 part of the circular economy concept. Recent studies have emphasized that waste-derived
112 resources can serve as valuable feedstocks for environmental and energy-related applications,
113 reducing disposal problems while creating economic and environmental benefits (Hassan et al.
114 2023, Li et al. 2025}. In this context, wheat straw represents an abundant agricultural residue that
115 can be converted into value-added biochar-based materials for wastewater treatment.

116 As a renewable natural resource, WS offers significant potential to produce biochar, which can
117 be utilized in various environmental applications. Biochar is a carbon-rich solid byproduct
118 produced through the pyrolysis of biomass at temperatures below 700°C. It can be derived from
119 a wide range of low-cost biomass sources, including manure (Cao et al. 2009), organic waste
120 (Kumar et al. 2016), bioenergy crops (e.g., grasses and willows) (Yrjälä and Zheng 2021), and
121 crop residues (Patel and Panwar 2023). Recent bioresource valorization studies have further
122 highlighted the environmental benefits of converting biomass into biochar and other value-added
123 products for sustainable applications (Tanweer et al. 2025). Biochar's physicochemical
124 properties, like a large surface area, high porosity, abundant oxygen-rich functional groups, and
125 notable cation exchange capacity, make it a highly effective adsorbent for wastewater treatment
126 in comparison to metal based adsorbent (Hussain et al. 2025; Johnston et al. 2021). The presence
127 of oxygenated functional groups on the biochar surface imparts a negative charge, facilitating the
128 adsorption of positively charged heavy metals and other pollutants from wastewater (Zhang et al.
129 2025). As a result, it is suitable for use as an adsorbent material to reduce the levels of heavy
130 metals in water. Additionally, biochar can reduce environmental pollution, enhance soil quality
131 (Kabir et al. 2023), promote sustainability (Afshar and Mofatteh 2024) and slow down climate
132 change (Shoudho et al. 2024). Numerous studies have demonstrated the effectiveness of biochar
133 as a cost-efficient and highly capable adsorbent for wastewater treatment, alongside its
134 applications in soil improvement.

135 Biomass-derived biochar has been widely proposed for the removal of various contaminants
136 from water, including organic pollutants, heavy metals, and nutrient pollutants (Elbagory et al.

137 2025; Liu et al. 2025; Ma et al. 2025; Olugbenga et al. 2024; Yan et al. 2025). Recent studies
138 have further demonstrated that biomass-derived porous carbon materials exhibit excellent
139 adsorption performance toward emerging contaminants due to their high surface area,
140 hierarchical pore structure, and abundant functional groups. For instance, lignin-derived
141 hierarchical porous carbon showed enhanced adsorption capacity for tetracycline, highlighting
142 the potential of biomass-based adsorbents for environmental remediation (Li et al. 2026). One of
143 the studies reported the removal of Cu^{2+} by WS biochar, which showed 6.6% at pH 4.5 and
144 20.12% at 8 g dose (Wang et al. 2022). However, W-S biochar is often limited by its surface
145 chemistry and adsorption capacity. To overcome these limitations, biochar modifications have
146 been explored to enhance its adsorption properties. One approach is to incorporate layered
147 double hydroxides (LDHs), such as calcium-magnesium-aluminum (Ca–Mg–Al) LDH, onto
148 biochar. LDHs are known for their high anion-exchange capacity, tunable composition, and
149 interlayered structure, which facilitate the adsorption of various contaminants (Kameliya et al.
150 2023). When combined with biochar, these properties may create a material with synergistic
151 effects.

152 As previously mentioned, WS a plentiful agricultural byproduct, offered a cheap and renewable
153 precursor for the creation of biochar. For Cu^{2+} ion adsorption under batch conditions, the Ca–
154 Mg–Al LDH modified wheat straw biochar (WsBio-LDH composite) was optimized. By
155 employing commonly used isotherms, such as Langmuir, Freundlich, and Temkin, as well as
156 kinetic models, such as pseudo-first-order (PFO) and pseudo-second order (PSO), the
157 mechanism of Cu^{2+} ion adsorption by the WsBio-LDH composite was examined. In order to
158 achieve optimal experimental settings, response surface methodology (RSM) with a central
159 composite design (CCD) were also used to determine optimal experimental conditions and
160 analyze the interactive effects of operational parameters.

161 This study contributes to ongoing research on sustainable adsorbent development for
162 environmental remediation. The present work explores the integration of Ca–Mg–Al layered
163 double hydroxides (LDHs) with wheat straw biochar to prepare a biomass-derived composite
164 adsorbent for Cu^{2+} removal. Response surface methodology based on central composite design
165 (RSM-CCD) is further applied to optimize key adsorption parameters and support the
166 interpretation of process–performance relationships. The increasing interest in sustainable

167 material engineering has extended across several environmental fields, including wastewater
168 remediation, carbon utilization, and clean energy production. Recent studies have emphasized
169 the role of tailored material structures and surface-active sites in enhancing environmental
170 performance. However, the combined use of wheat straw biochar and Ca–Mg–Al LDHs for Cu²⁺
171 removal under statistically optimized conditions remains relatively underexplored. Therefore,
172 this study aims to address this gap by preparing a wheat straw biochar-supported Ca–Mg–Al
173 LDH composite and evaluating its adsorption performance through a systematic RSM-CCD
174 approach.

175 **Materials and Methods**

176 *Synthesis of LDH W-S Biochar Composite*

177 The co-precipitation method was used to prepare the composite adsorbent of CaMgAl(LDH) and
178 WS biochar. To prepare the LDH of CaMgAl, 5.90 g (0.5 M) of calcium nitrate tetrahydrate
179 Ca(NO₃)₂·4H₂O, 6.025 g (0.5 M) of aluminum nitrate nonahydrate Al(NO₃)₃·9H₂O, and 6.41 g
180 (0.5 M) of magnesium nitrate hexahydrate Mg(NO₃)₂·6H₂O were dissolved in 50 mL of
181 deionized water in a beaker. The mixture was stirred continuously for about an hour to ensure
182 complete dissolution of the salts. Once dissolved, the solution was transferred to another beaker
183 containing 5 g of WS biochar, and the mixture was stirred continuously. A solution of NaOH
184 (0.42 g) and Na₂CO₃ (0.58 g) in 100 mL of deionized water was then added dropwise via a
185 burette until the pH of the solution reached approximately 10. The resulting slurry was stirred for
186 an additional two hours. Afterward, the slurry was transferred to a centrifuge tube and
187 centrifuged at 6000 rpm to separate the particles. This washing step was repeated five times
188 using deionized water. Following the washing procedure, the composite material was dried in an
189 oven at 85°C for 24 hours.

190 *Batch Adsorption Experiment*

191 Batch adsorption experiments were performed to evaluate the removal of Cu²⁺ from aqueous
192 solution using the WsBio-LDH composite as an adsorbent. Stock solutions of Cu²⁺ were
193 prepared at a concentration of 20 ppm. For each experiment, an appropriate dose of the adsorbent
194 (0.4 g) was added to 40 mL of the Cu²⁺ solution in a flask. The pH of the solutions was adjusted
195 to 6.0 using 0.1 M HCl and 0.1 M NaOH, as needed (Mondal 2009). The mixture was

196 mechanically shaken at a speed of 200 rpm at ambient temperature (25°C) using an orbital
197 shaker to ensure uniform mixing. At regular time intervals, the residual concentrations of Cu²⁺ in
198 the solutions were analyzed using the Atomic Absorption Spectrometer. The residual Cu²⁺
199 concentration at time (*t*) was calculated using the following equation:

$$200 \quad q_t = \frac{C_0 - C_t}{m} \times V \quad (1)$$

201 In this equation, *V* (mL) represents the volume of solution, and *m* (g) corresponds to the mass of
202 the WsBio-LDH composite. 'C₀' is the initial metal ion concentration (mg/L), 'C_t' is the metal
203 concentration at time *t* (mg/L) (Bayantong et al. 2021).

204 The % removal efficiency of the adsorption process was calculated using Equation 2.

$$205 \quad \% \text{ removal} = \frac{C_0 - C_t}{C_0} \times 100 \quad (2)$$

206 Other batch parameters were also tuned, including the dose of the WsBio-LDH combination, the
207 starting concentration of Cu²⁺, and the pH of the solution. Isotherms and kinetic models were
208 used to examine the WsBio-LDH composite's chemical and physical surface properties as well as
209 Cu²⁺ molecules' affinity for the adsorbent's surface coverage. The adsorption of Cu²⁺ was
210 investigated using the Langmuir, Freundlich, and Temkin isotherm models, which looked at the
211 interactions between the adsorbent and the investigated metal ions at various concentrations.

212 ***Isotherm Models***

213 The linear representation of the Freundlich isotherm is depicted in Equation 3, where *K_f*
214 represents the Freundlich constant and 1/*n* denotes the adsorption intensity, which depends on the
215 heterogeneous nature of the nanocomposite (Cheung et al. 2007a; Liu and Wang 2013a). The
216 Freundlich isotherm is formulated under the assumption of a heterogeneous surface (Othman et
217 al. 2023) with a non-uniform distribution of active sites over the surface through a multilayer
218 adsorption process. The value of 1/*n* determines the isotherm type, in which 1/*n* = 0, 0 < 1/*n* < 1,
219 and 1/*n* > 1 indicate irreversible, favorable, and unfavorable adsorption, respectively.

$$220 \quad \log q_e = \log K_f + \frac{1}{n} \log C_e \quad (3)$$

221 The Freundlich isotherm equation was applied to describe multilayer adsorption on
222 heterogeneous surfaces (Cheung et al. 2007b; Liu and Wang 2013a). According to the Langmuir

223 model, the surface of the adsorbent possesses a predetermined number of active sites where the
224 adsorbate can adhere to form a monolayer. Once a monolayer has formed, no additional
225 adsorbate can adhere to the surface. The linear form of the Langmuir model is shown in Equation
226 4. C_e (mg/L) shows the liquid phase concentration, where q_e (mg/g) denotes the adsorption
227 capacity of the WsBio-LDH composite at equilibrium. By plotting $1/q_e$ against $1/C_e$, it is
228 possible to obtain the value of K_L . K_L (L/g) is the Langmuir isotherm constant, and q_{max} signifies
229 the maximum adsorption capacity related to the area occupied by a monolayer of adsorbate.

$$230 \quad \frac{1}{q_e} = \left(\frac{1}{K_L q_{max}} \right) \frac{1}{C_e} + \frac{1}{q_{max}} \quad (4)$$

231 The Langmuir model assumes monolayer adsorption on a homogeneous surface with finite
232 adsorption sites (Liu and Wang 2013b). Unlike the Langmuir isotherm, the Temkin isotherm
233 assumes that adsorption energy decreases linearly as adsorbent-adsorbate interaction increases
234 and more surface of the adsorbent is covered with adsorbate molecules. Equation 5 represents the
235 linear form of the Temkin isotherm model, where $B = RT/b$, b (KJ/mol) represents the Temkin
236 constant, R is known as the universal gas constant (8.314 J mol⁻¹ per kelvin), B shows the heat
237 of adsorption (J/mol), and A is the Temkin constant.

$$238 \quad q_e = \frac{RT}{B_T} \ln A_T + \frac{RT}{B_T} \ln C_e \quad (5)$$

239 The Temkin model considers adsorbent adsorbate interactions and a linear decrease in adsorption
240 energy (Othman et al., 2023).

241 ***Kinetic Models***

242 The kinetics of adsorption is known as the key to understanding how quickly an adsorbent can
243 capture an adsorbate (metal) from a solution. Various kinetic models are used to interpret the
244 experimental adsorption data and determine the rate-limiting step.

245 The PFO model assumes that the adsorption rate is directly proportional to the number of
246 unoccupied active sites on the adsorbent. This model is typically applicable to systems where
247 physisorption is the dominant adsorption mechanism. The linear form of the PFO model is
248 expressed in Equation 6

$$249 \quad \log q_e - q_t = \log q_e - \frac{k_1}{2.303} t \quad (6)$$

250 Here, k_1 is the PFO rate constant (min^{-1}), q_t is the quantity of metal ion adsorbed at time t
251 (mg/g), and q_e is the amount of adsorbate adsorbed at equilibrium (mg/g).

252 Physisorption-controlled adsorption processes were described by the pseudo-first-order kinetic
253 model (Cheung et al., 2007).

254 According to the PSO model, the square of the number of vacant sites determines the rate of
255 adsorption. It is frequently employed in chemisorption procedures, in which the adsorbent and
256 adsorbate form chemical bonds. Equation 7 represents the PSO model linear form.

$$257 \quad \frac{t}{q_t} = \frac{1}{k_2 q_e^2} + \frac{t}{q_t} \quad (7)$$

258 Here, K_2 is the PSO rate constant ($\text{g}/(\text{mg}/\text{min})$). The pseudo-second order kinetic model assumes
259 chemisorption as the rate-limiting step (Othman et al., 2023).

260 ***Characterization Techniques***

261 Characterization techniques used for the WsBio-LDH composite adsorbent include Fourier
262 transform infrared (FTIR) spectroscopy, the energy dispersive X-ray (EDX) spectroscopy, and
263 scanning electron microscopy (SEM) to investigate the surface functional groups and
264 morphological changes. FTIR analysis was specifically employed to identify the chemical bonds
265 and functional groups present on the surface of the WsBio-LDH composite adsorbent (Haleem et
266 al. 2022), both before and after Cu^{2+} adsorption. SEM and EDX provided a few insights into the
267 surface morphology (Obey et al. 2022), revealing structural changes and the adsorption of metal
268 ions, which helped in assess the effectiveness of the WsBio-LDH composite adsorbent in
269 removing Cu^{2+} from aqueous solution

270 ***Response Surface Methodology***

271 The RSM was used to systematically optimize and assess the relationship between adsorption
272 efficiency (response) and the impact of various parameters on the Cu^{2+} removal efficiency of the
273 WsBio-LDH composite (Abdipour and Hemati 2024; Jafari et al. 2025; Torabideh et al. 2025) .
274 A quadratic relationship in RSM was constructed using a three-factor CCD. Factorial, axial, and
275 center points are all combined in this model. As indicated in Table 1, the main independent
276 factors (along with coded levels) include contact duration, dose of the WsBio-LDH combination,
277 solution pH, and Cu^{2+} concentration, which were examined for their effects on removal

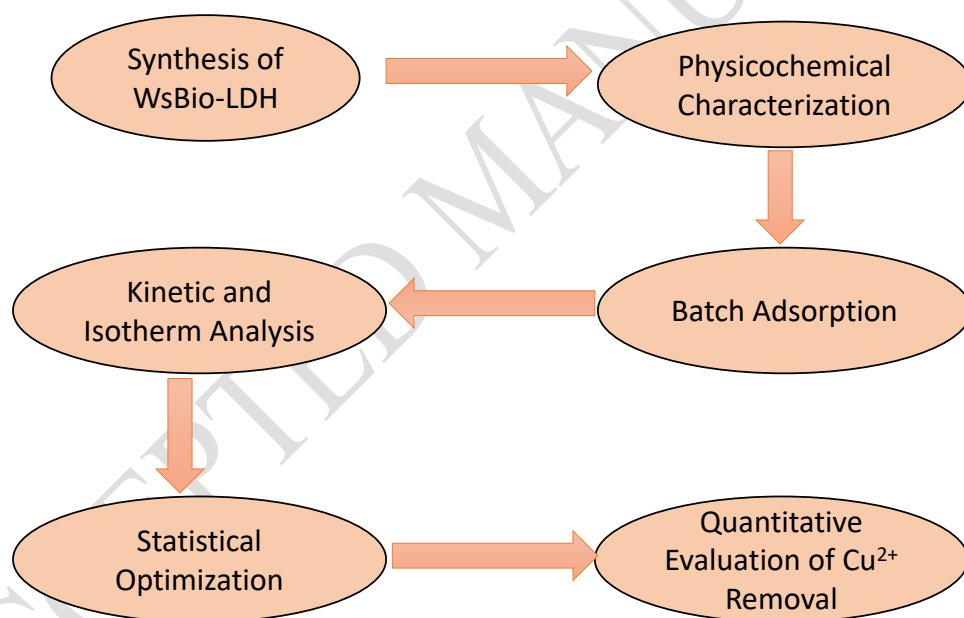
278 efficiency. WsBio-LDH The effects of both individual variables and their interactions on the
279 Cu^{2+} removal efficiency of WsBio-LDH composite's was evaluated.

280 **Table 1: Independent variables and their coded levels**

Independent variables	Units	+1	0	-1
T	min	1	60.5	120
LDH/W.B. Dose	g/L	0.05	0.325	0.6
pH		2	4	6
Cu^{+2} Conc.	mg/L	5	37.5	70

281 **Workflow of the Proposed Experimental Optimization Model**

282 The proposed study follows a systematic workflow comprising:



283

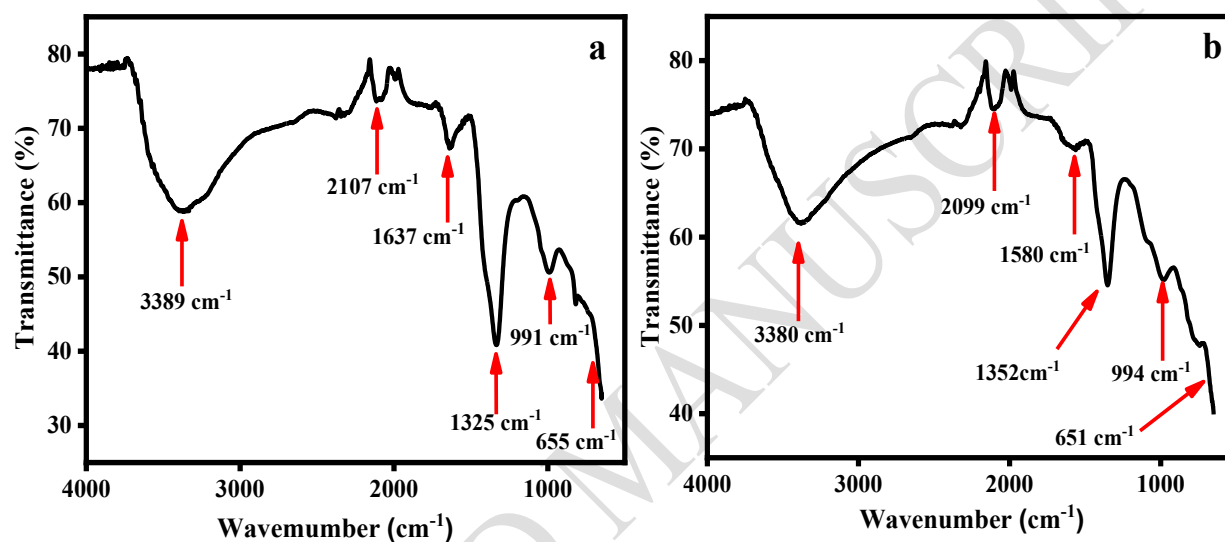
284 **Workflow for the removal of Cu^{+2}**

285 **Results and Discussions**

286 ***FTIR Spectroscopy***

287 The FTIR spectra of the WsBio-LDH composite before and after Cu^{2+} adsorption are presented
288 in Figure 1, illustrating the changes in surface functional groups. The bands seen at 3389 and

289 1637 cm^{-1} are linked to the typical -OH stretching vibrations and the bending vibrations of H_2O
290 (Xu et al. 2020). These are related to the hydroxyl groups found in the adsorbent, as well as the
291 water that is either adsorbed or located between the layers of the sorbent. The characteristic
292 peaks at 2093 cm^{-1} indicate the presence of $\text{C}\equiv\text{C}$ or $\text{C}\equiv\text{N}$ stretching vibrations, suggesting
293 unsaturated alkyne. The sharp peaks at 1328 and 991 cm^{-1} were allocated to the asymmetric
294 stretching vibration mode of $\text{C}-\text{O}$ in CO_3^{2-} and stretching of $\text{C}-\text{O}$, respectively (Adachi-Pagano
295 et al. 2003; Zou et al. 2017).



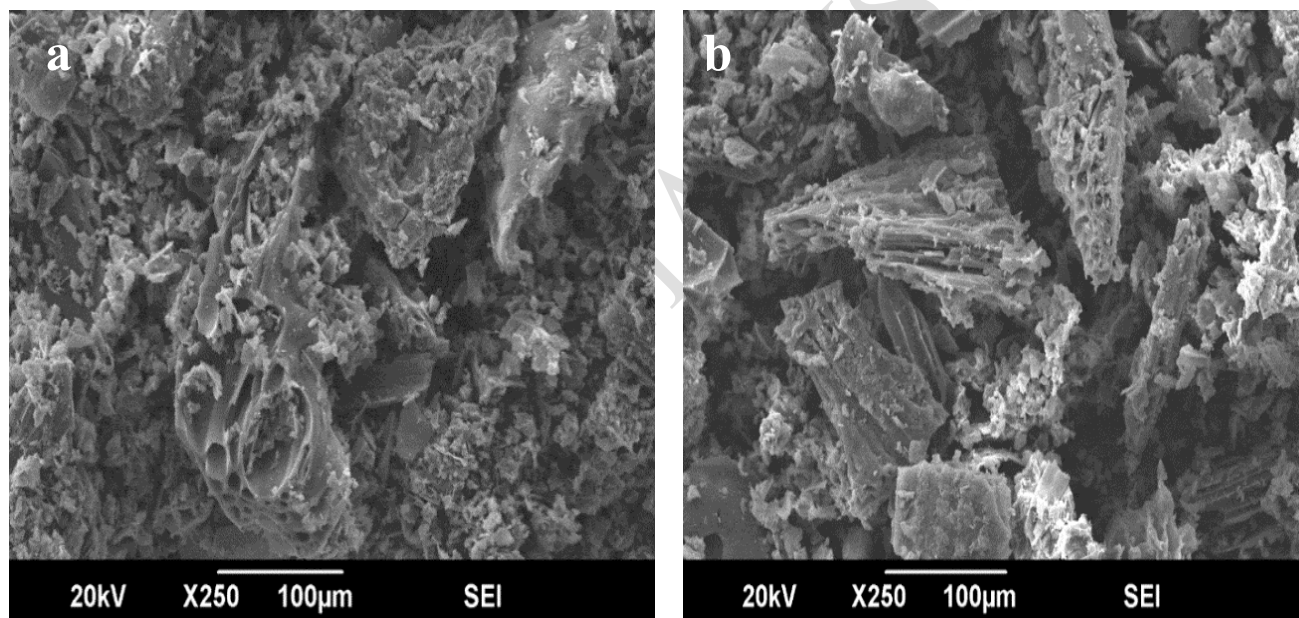
296
297 **Figure 1.** Fourier transform infrared spectra of (a) the WsBio-LDH composite, and (b) the
298 WsBio-LDH composite after Cu^{2+} adsorption.

299 The bands about 655 cm^{-1} are associated with M-OH or M-O stretching vibrations, where M
300 represents Mg, Al, or Ca. The relationships between cations and oxygen are defined by these
301 bands (Frost and Klopogge 1999). Following the Cu^{2+} adsorption, the FTIR spectra of the
302 WsBio-LDH composite exhibit a discernible shift, as shown in Figure 1b. Cu^{2+} was successfully
303 adsorbed onto the surface of the WsBio-LDH composite adsorbent, as evidenced by the shift of
304 all the bands and the narrowing of the OH band. The signal at 1637 cm^{-1} is reduced and shifted
305 to 1580 cm^{-1} by the Cu^{2+} interaction, indicating a decrease in hydroxyl frequency (Chen et al.
306 2024). The consumption of hydroxyl groups during the adsorption process could be attributed to
307 the formation of Cu-OH on the surface of the WsBio-LDH composite (Lyu et al. 2023).

308

309 **Scanning Electron Microscopy**

310 Figure 2 illustrates the use of SEM and EDX analyses to examine the surface shape and
311 elemental composition of the WsBio-LDH composite before and after Cu^{2+} adsorption. SEM
312 imaging enables visualization of surface modifications, facilitating a better understanding of
313 morphological changes (Rydz et al. 2019). As seen in Figure 2a (Shiriazar et al. 2022), SEM
314 scans revealed a rough surface of the WsBio-LDH composite that primarily contained two
315 separate phases: the raw biochar and micro-sized Ca/Al/Mg-LDH particles scattered over it. Cu^{2+}
316 is successfully adsorbed into the WsBio-LDH composite adsorbent, as seen in Figure 2b, where
317 the holes become saturated with Cu^{2+} and the surface of the WsBio-LDH composite appears
318 rougher.



319

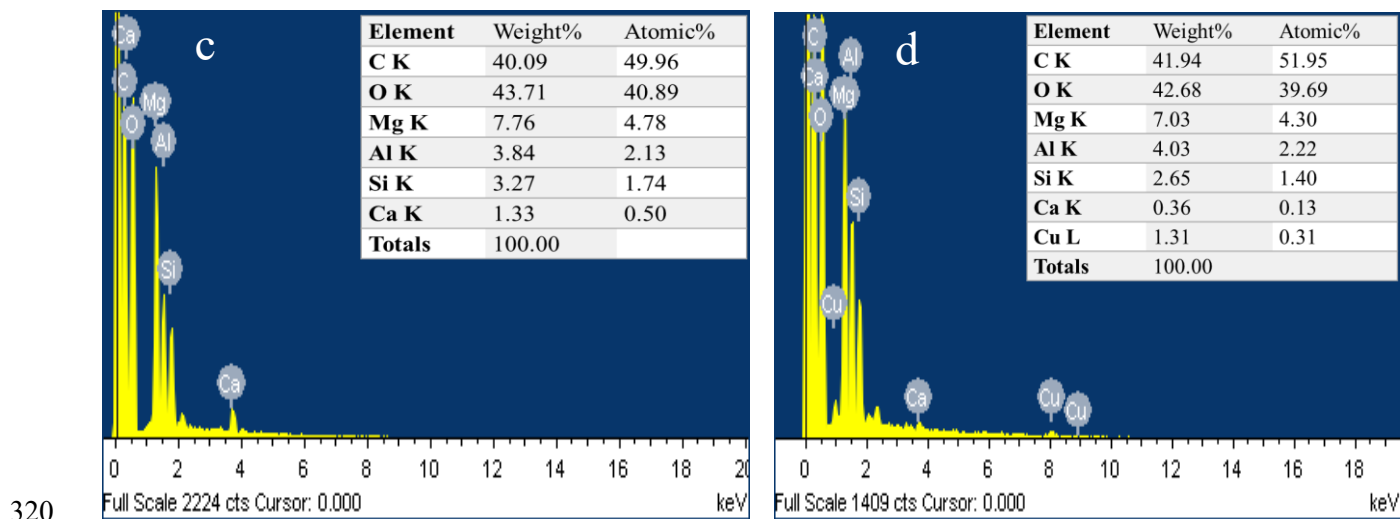


Figure 2. SEM images of (a) the WsBio-LDH composite, and (b) the WsBio-LDH composite after Cu^{2+} adsorption. EDX spectra of (c) the WsBio-LDH composite and (d) the WsBio-LDH composite after Cu^{2+} adsorption.

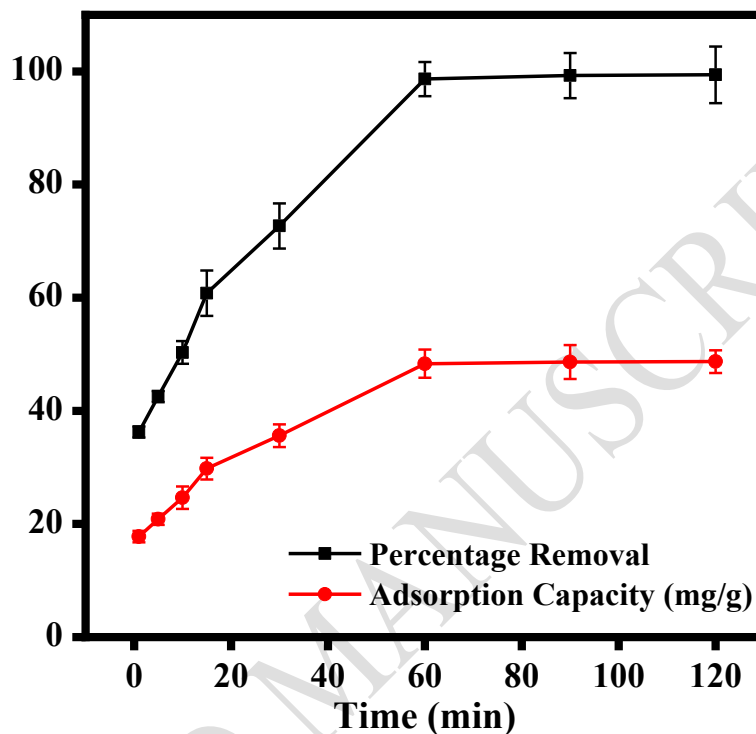
EDX spectroscopy showed the elemental composition of the WsBio-LDH composite before and after adsorption of Cu^{2+} (Nzediegwu et al. 2021). As shown in Figure 2c, an increase in oxygen content (70.62 wt%) and a reduction in carbon content (17.07 wt %) were observed, implying successful adsorption and surface modification. Furthermore, in the WsBio-LDH composite, peaks corresponding to Ca, Al, and Mg confirmed successful inclusion of these elements. Subsequently, the WsBio-LDH composite displayed changes in elemental distribution and the presence of Cu^{2+} ions (Figure 2d), which demonstrates the interactions between the Cu^{2+} and the surface of the WsBio-LDH composite.

332 *Effect of Adsorption Parameters*

333 **Effect of the Contact Time**

334 Figure 3 illustrates the effect of contact time on Cu^{2+} removal efficiency and adsorption capacity
 335 of the WsBio-LDH composite. Determination of contact time aims to get the optimum time to
 336 adsorb contaminants. In this study, time variations were used as 1, 5, 10, 15, 30, 60, 100, and 120
 337 minutes, and the effect of contact time was studied at room temperature along with 0.4 g of the
 338 WsBio-LDH composite adsorbent for Cu^{2+} removal. Figure 3 shows that the WsBio-LDH
 339 composite revealed better performance, achieving 98.6% removal at 60 minutes, which increased
 340 slightly to 99% at 120 minutes. These results clearly indicate that the WsBio-LDH composite is

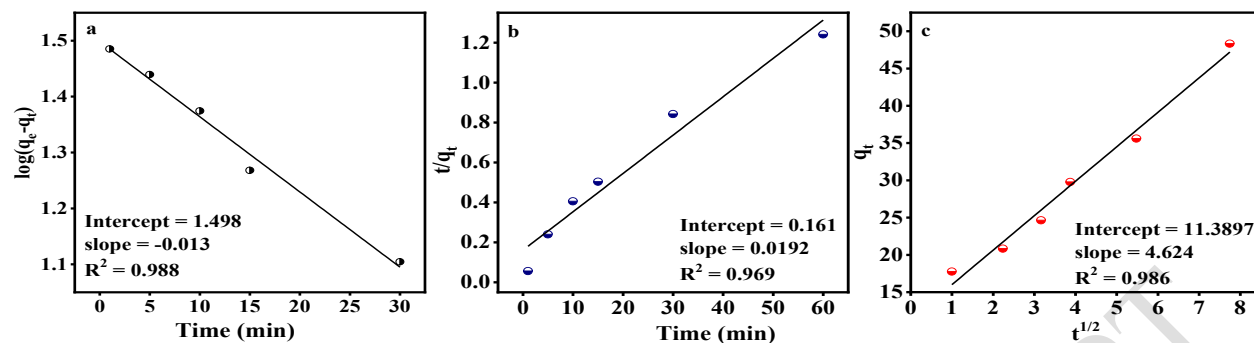
341 significantly more effective for Cu^{2+} removal. Therefore, 60 minutes contact time was selected
342 as the optimum time for further experiments, i.e., pH, Cu^{2+} concentration, and dose effect on
343 %age removal of the studied adsorbate (Cu^{2+}).



344
345 **Figure 3.** Effect of the contact time on the adsorption capacity and % removal of the WsBio-
346 LDH composite for Cu^{2+} ions from aqueous solution.

347 It should be noted that the contact-time experiment was conducted independently to determine the
348 equilibrium behavior of the adsorption process under fixed operating conditions. Although Cu^{2+} removal
349 reached approximately 98.6% within 60 min, the RSM optimization considered the simultaneous
350 interactions among contact time, adsorbent dosage, solution pH, and initial Cu^{2+} concentration.
351 Consequently, the statistically optimized contact time predicted by the RSM model was 87.06 min, which
352 corresponds to the maximum overall removal efficiency obtained when all process variables were
353 optimized together. Therefore, the values of 60 min and 87.06 min are not contradictory but represent
354 single-factor and multi-factor optimization outcomes, respectively.

355 The adsorption kinetics of Cu^{2+} onto the WsBio-LDH composite were analyzed using pseudo-
356 first-order (PFO), pseudo-second-order (PSO), and intraparticle diffusion (IPD) models, as
357 presented in Figure 4, with the corresponding kinetic parameters summarized in Table 2.



358

359 **Figure 4.** Kinetic model analysis for the WsBio-LDH composite (a) PFO, (b) PSO, (c) IPD.

360 The adsorption kinetics of Cu^{2+} onto the WsBio-LDH composite were evaluated using both
 361 pseudo-first-order (PFO) and pseudo-second-order (PSO) models. The PFO model exhibited a
 362 slightly higher coefficient of determination ($R^2 = 0.988$) compared with the PSO model ($R^2 =$
 363 0.969), indicating a better statistical fit to the experimental data. Therefore, based solely on the
 364 R^2 values, the PFO model more accurately describes the adsorption kinetics. However, the
 365 relatively high R^2 values obtained for both models suggest that the adsorption process may
 366 involve contributions from both physical and chemical interactions between Cu^{2+} ions and the
 367 WsBio-LDH surface. The observed agreement with the pseudo-first-order model suggests that
 368 physisorption may contribute significantly to the adsorption process. Similar adsorption behavior
 369 governed by physical interactions has been reported for pollutant adsorption systems involving
 370 surface-mediated adsorption mechanisms (Qin et al. 2023).

371 **Table 2.** Kinetic model parameters for adsorption of Cu^{2+} on WsBio-LDH composite.

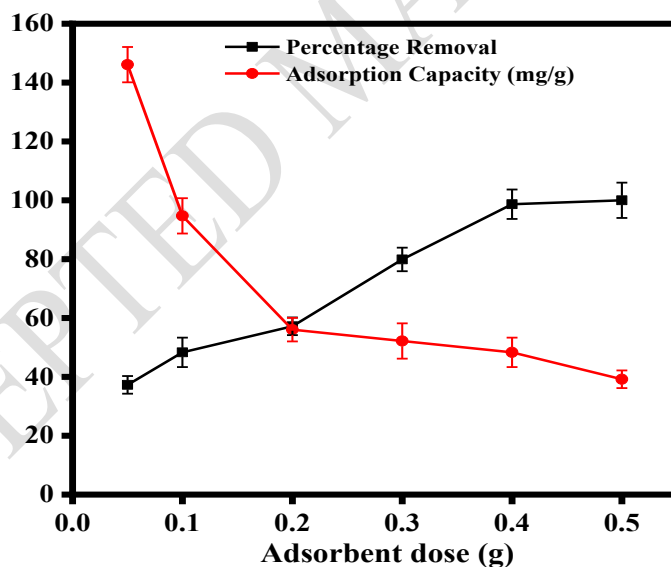
Kinetic models	Parameters	Values for the WsBio-LDH composite
PFO	K_1	0.03
	q_{exp}	48.3
	q_{cal}	52.63
	R^2	0.986
PSO	K_2	0.0022
	q_{exp}	48.3
	q_{cal}	52.63
	R^2	0.969
IPD	I	11.39

k_{diff}	4.62
R^2	0.988

372

373 **Effect of the Adsorbent Dose**

374 Figure 5 illustrates the effect of WsBio-LDH composite dose on the adsorption capacity and
 375 removal efficiency of Cu^{2+} . The adsorbent dosage regulates the accessibility of adsorption (Wang
 376 et al. 2020). The adsorbent's dosage was adjusted in increments of 0.1 g between 0.05 and 0.6 g
 377 under the following conditions: at an initial pH of 6, a contact period of 60 minutes, a shaking
 378 speed of 200 rpm, and room temperature. Figure 5 illustrates how the proportion of Cu^{2+} ions
 379 eliminated increased with an increase in adsorbent dosage. As seen, the percentage removal of
 380 Cu^{2+} reached 98% at 0.4 g of adsorbent used and increased to 100% at 0.6 g for the WsBio-LDH
 381 combination. These results demonstrate that increasing the adsorbent dosage enhances the
 382 adsorption efficiency, likely due to the increased accessibility of active adsorption sites.

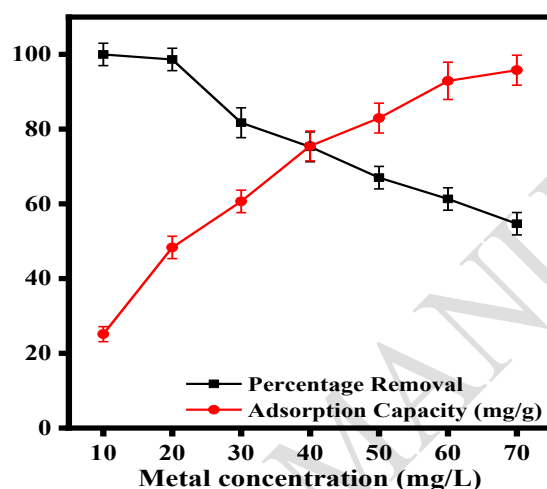


383
 384 **Figure 5.** Effect of the WsBio-LDH composite dose on the adsorption capacity and Cu^{2+} %
 385 removal.

386 **Effect of the Cu^{2+} Concentration**

387 Figure 6 show that the initial Cu^{2+} concentration affects the WsBio-LDH composite adsorption
 388 ability. Figure 6 shows the percentage removal of Cu^{2+} metal ions for the WsBio-LDH

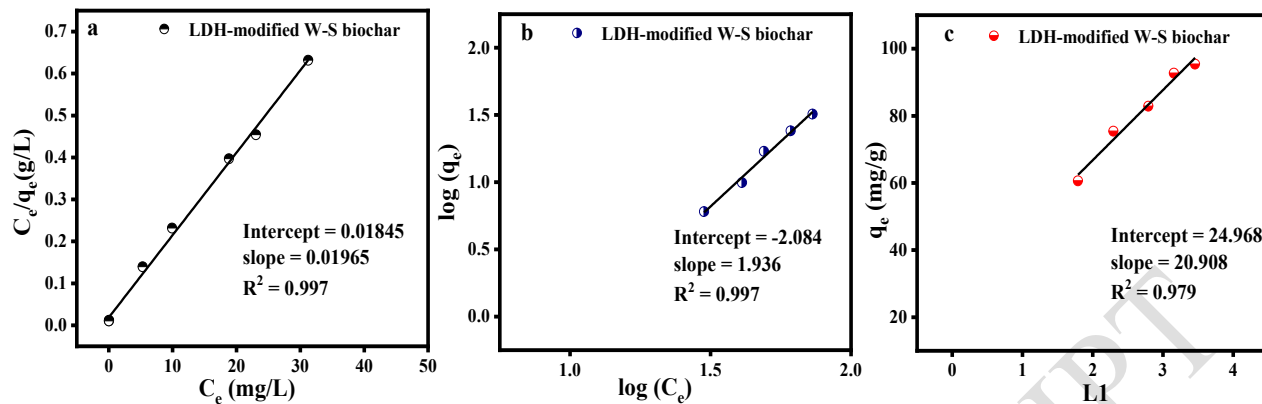
389 composite adsorbent at different starting concentration levels ranging from 5 to 70 mg/L. The
390 results indicate that as the concentration of the adsorbate increased, the percentage removal of
391 the metal ions under study decreased. The accessible empty binding sites on the adsorbent's
392 surface are responsible for the increased Cu^{2+} absorption at lower concentrations. The increased
393 Cu^{2+} metal ion in the aqueous phase results in competition and saturation on the adsorbent
394 surface, which is responsible for the decrease in the percentage of metal removal. Thus, mass
395 transfer is hampered (El-Shafey et al. 2024).



396
397 **Figure 6.** Effect of initial Cu^{2+} concentrations on the adsorption capacity and % removal of Cu^{2+}
398 using the WsBio-LDH composite as an adsorbent.

399 *Adsorption isotherms*

400 The adsorption behavior of Cu^{2+} onto the WsBio-LDH composite was evaluated using Langmuir,
401 Freundlich, and Temkin isotherm models, as shown in Figure 7, with the corresponding isotherm
402 parameters summarized in Table 3. The Langmuir model provided the best fit, with a higher R^2
403 value of 0.997 for the WsBio-LDH composite. Additionally, the adsorption capacity increased,
404 as seen in Table 3 for the WsBio-LDH composite, indicating that the modification has enhanced
405 the adsorption efficiency, and the adsorption process follows a monolayer adsorption
406 mechanism.



407
 408 **Figure 7.** Adsorption isotherms: (a) Langmuir isotherm, (b) Freundlich isotherm, and (c) Temkin
 409 isotherm for Cu²⁺ adsorption on the WsBio-LDH composite.

410 The Freundlich model, although showing a good R² value of 0.989, does not fit the adsorption
 411 behaviors as accurately as the Langmuir model in this case. The Temkin model is less suitable
 412 for the WsBio-LDH composite adsorbent, especially when compared to the better fits provided
 413 by Langmuir and the Freundlich models. In conclusion, the Langmuir model is the best fit, with
 414 an increase in adsorption capacity, demonstrating a more favorable monolayer adsorption
 415 process for the WsBio-LDH composite.

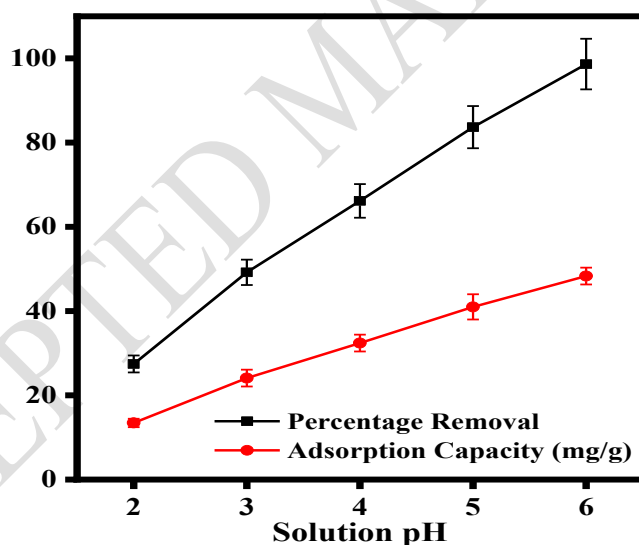
416 **Table 3.** Isotherm model parameters of Cu²⁺ adsorption on WsBio-LDH composite.

Isotherm models	Parameters	Values for the WsBio-LDH composite
Langmuir	q _{exp}	95.79
	q _{max}	100.00
	R _L	0.02
	R ²	0.997
Freundlich	K _f	86.10
	n	2.084
	R ²	0.989
	B	120.54

	LN(AT)	1.194
Temkin	R ²	0.979

417 **Effect of the solution pH**

418 Figure 8 illustrates the effect of solution pH on the Cu²⁺ removal efficiency of the WsBbio-LDH
 419 composite at pH values ranging from 2 to 6. Using the WsBio-LDH composite as an adsorbent,
 420 98.6% of the Cu²⁺ was removed at pH 6. This significant improvement in performance highlights
 421 the WsBio-LDH composite's greater adsorption capacity and outstanding efficacy in Cu²⁺
 422 removal across the pH range. The percentage of metal ions removed increases as pH rises,
 423 according to similar findings reported in the literature (Wang et al. 2013). An increase in the
 424 percent removal at higher pH is due to less competition by H⁺ ions and more efficient de-
 425 protonation of functional groups on the surface of the WsBio-LDH composite for copper ion
 426 binding.



427
 428 **Figure 8.** Effect of pH on the adsorption capacity and % removal of Cu²⁺ using the WsBio-LDH
 429 composite adsorbent.

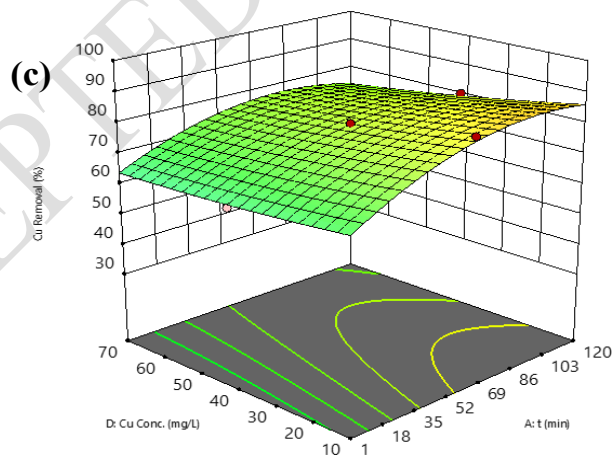
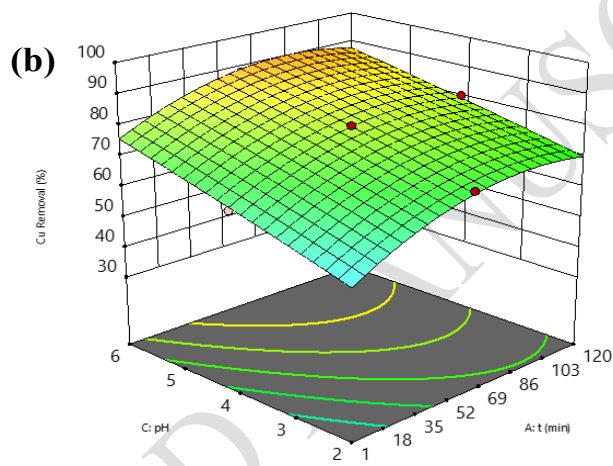
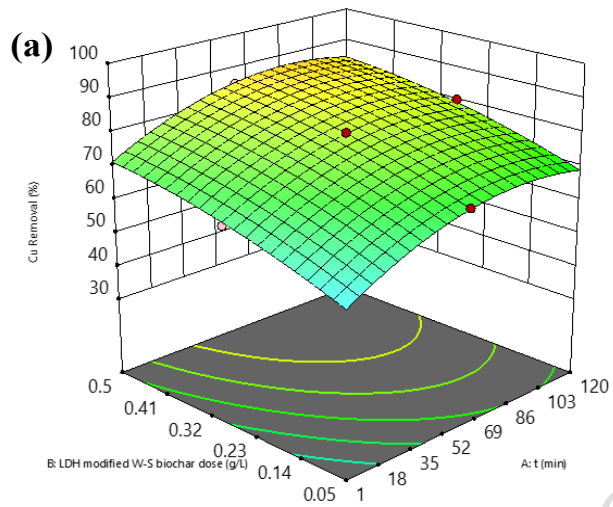
430 **RSM Analysis of the WsBio-LDH composite vs Cu²⁺ Adsorption**

431 Response surface methodology was employed to investigate the interactive effects of contact
 432 time, adsorbent dosage, solution pH, and initial Cu²⁺ concentration on removal efficiency
 433 (Figures 9 and 10). ANOVA results revealed that pH and adsorbent dosage had the most

434 significant positive effects on Cu^{2+} removal efficiency, whereas initial metal concentration
435 negatively impacted removal due to active site saturation. To visualize these effects and their
436 interactions, three-dimensional response surface plots and corresponding contour plots were
437 generated. These graphical representations provide critical insights into the adsorption behavior
438 of the WsBio-LDH composite for Cu^{2+} under varying experimental conditions. Figure 9 (a, b, c)
439 illustrates how changes in the four independent variables, contact time, adsorbent dosage,
440 solution pH, and initial Cu^{2+} concentration influence the overall removal efficiency.

441 **1. Effect of the Contact Time and the WsBio-LDH composite Dose**

442 The three-dimensional surface plots and two-dimensional contour diagrams reveal how contact
443 time and adsorbent dosage work together to enhance Cu^{2+} removal. When both parameters are
444 increased, the removal efficiency rises substantially, reaching approximately 90–99% at optimal
445 conditions. Initially, extending the contact duration allows more Cu^{2+} ions to interact with the
446 available active sites on the WsBio-LDH composite surface. This extended interaction period
447 facilitates adequate time for both mass transfer processes and chemical adsorption to occur.
448 Simultaneously, increasing the amount of WsBio-LDH composite introduces additional binding
449 sites into the system. However, the response curves begin to level off at higher adsorbent
450 quantities and prolonged contact periods, suggesting that saturation has been achieved. Beyond a
451 certain threshold, adding more adsorbent or extending the contact time yields minimal
452 improvement in removal performance, likely because active sites begin to overlap or the system
453 reaches equilibrium. These observations align with established adsorption kinetic principles and
454 highlight the effectiveness of LDH functionalization in enhancing the available surface area for
455 adsorption.



456

457 **Figure 9.** RSM of the interaction between (a) t (min) and the WsBio-LDH composite dose (g),

458 (b) t (min) and pH, and (c) t (min) and Cu^{2+} concentrations (mg/L) on Cu^{2+} removal (%).

459

460

461 **2. Effect of Contact Time and solution pH**

462 Figure 9b illustrates a interactive effect of pH and contact time. The adsorption efficiency
463 dramatically rises up to roughly 6, after which the curve flattens. At lower pH values (acidic
464 media), the removal efficacy is reduced due to competition between H^+ and Cu^{2+} ions for
465 adsorption sites. As pH approaches neutral, there is less competition and more negative charge
466 density on the adsorbent surface, which promotes Cu^{2+} binding via electrostatic attraction and
467 surface complexation.

468 When combined with extended contact time, this optimal pH range (5.5-6.5) enables nearly
469 complete Cu^{2+} removal, underscoring the importance of surface chemistry and ionic equilibrium.
470 It is crucial to carefully interpret pH measurements over 7 in these systems because Cu^{2+}
471 precipitates as hydroxides at pH 7, which may impede the actual adsorption mechanism.

472 **3. Effect of Contact Time and Initial Cu^{2+} Concentration**

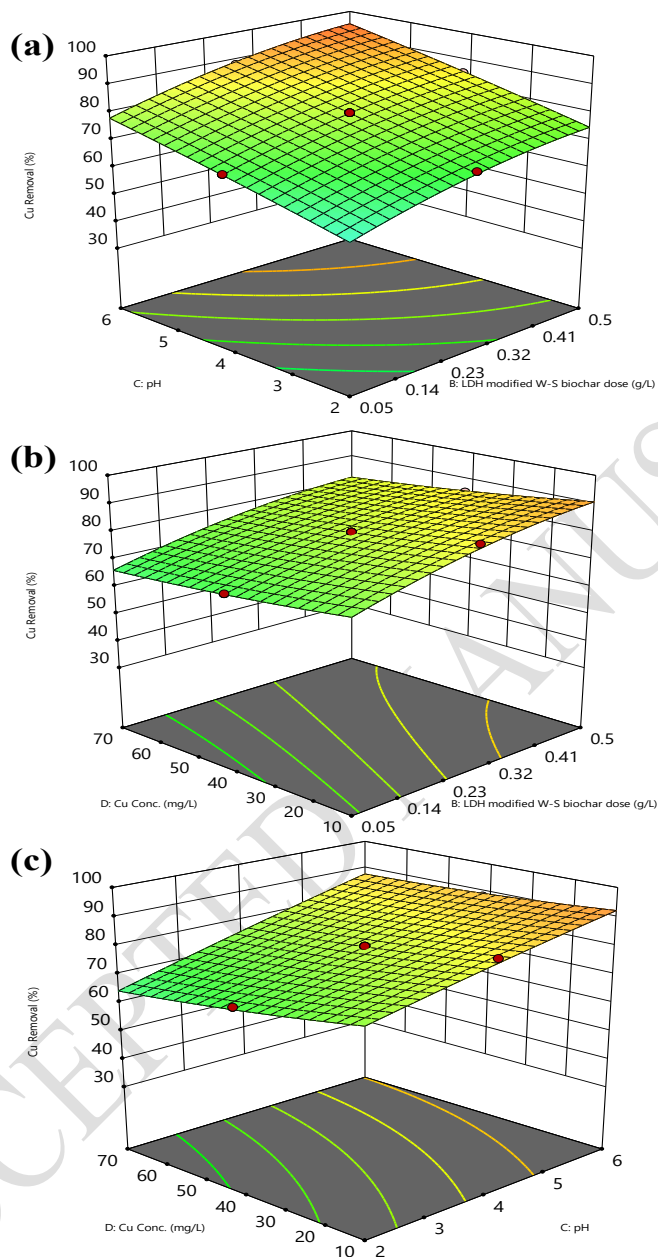
473 Particularly at shorter contact durations, this collection of graphs shows an inverse connection
474 between Cu^{2+} concentration and removal efficiency. Cu^{2+} ions compete more fiercely for a small
475 number of adsorption sites as the initial metal concentration rises. This lowers removal efficiency
476 at shorter contact times by limiting the number of active sites available for all ions.

477 Longer contact times, however, bring the system closer to adsorption equilibrium, allowing for
478 improved removal even at larger concentrations. However, because the adsorbent surface
479 eventually becomes saturated, achieving maximum efficiency is more difficult than with lower
480 concentrations. For optimal treatment efficacy, these graphs highlight the necessity of optimizing
481 both contact time and Cu^{2+} loading.

482 **4. Effect of the solution pH and the WsBio-LDH composite Dose**

483 The removal of Cu^{2+} is significantly impacted by the pH-adsorbent dosage relationship. The
484 elimination is extremely sensitive to pH variations at low dosages. The elimination is much
485 increased by raising the pH from 3 to about 6, which supports the process of improved surface
486 ionization and electrostatic contact. Because there are many surface locations to compensate for
487 less-than-ideal ionic conditions, higher dosages lessen the system's sensitivity to pH.
488 Interestingly, Peak removal occurs at pH 6 at an adsorbent dosage of 0.5 g, as shown in Figure

489 10a. This result represents an optimal equilibrium in which electrostatic interactions, surface
490 area, and ion exchange capacity are all maximized.



491
492 **Figure 10.** RSM of the interaction between (a) pH and the WsBio-LDH composite dose (g), (b)
493 Cu^{2+} concentrations (mg/L) and the WsBio-LDH composite dose (g), and (c) Cu^{2+} concentration
494 (mg/L) and pH on Cu^{2+} removal (%).

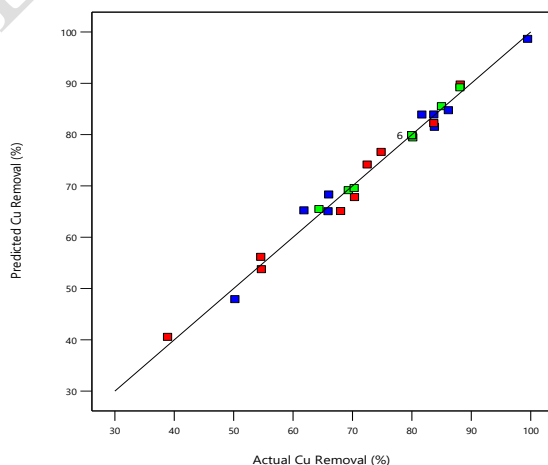
495
496

497 **5. Effect of the solution pH and Initial Cu²⁺ Concentration**

498 The prominence of pH as a crucial parameter is further demonstrated by the contour and surface
499 plots for pH and Cu²⁺ concentration (Figure 10b). Regardless of Cu²⁺ concentration, elimination
500 improves with increasing pH. However, the effect is stronger at lower concentrations. This
501 implies that when it comes to regulating the adsorption behavior, pH-mediated surface charge
502 alterations are more important than concentration effects. Due to a lack of active sites and strong
503 competition from H⁺ ions, the system performs poorly at low pH and high Cu²⁺ levels. On the
504 other hand, almost total elimination is shown at ideal pH and lower Cu²⁺ concentrations,
505 confirming the need for pH regulation in real-world applications.

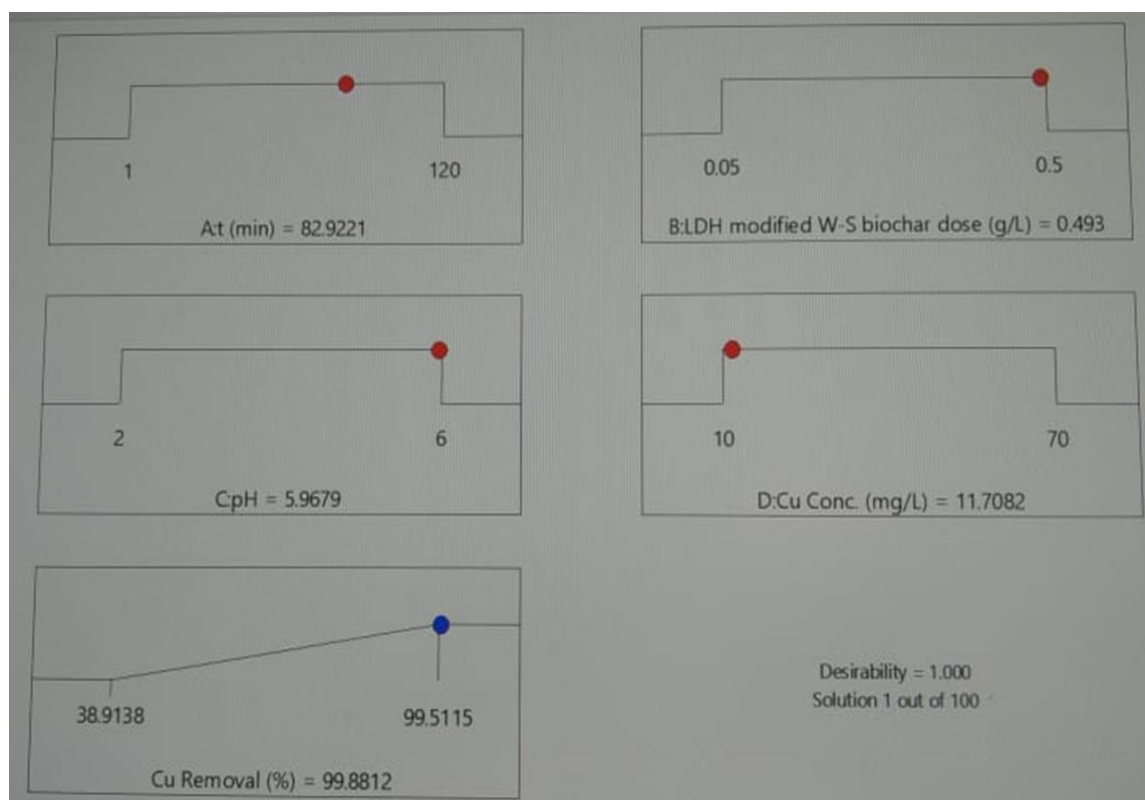
506 **6. Effect of the WsBio-LDH composite Dose and Cu²⁺ Concentration**

507 The antagonistic relationship between Cu²⁺ concentration and adsorbent dose is depicted in the
508 last set of graphs (Figure 10c). As anticipated, removal efficiency increases with increasing dose,
509 whereas it tends to decrease with rising Cu²⁺ concentration. A higher dose, on the other hand,
510 efficiently counteracts the adverse effects of high concentrations by providing more adsorption
511 sites and protecting the system against abrupt saturation. The system's nonlinear behavior is
512 highlighted by the response surface's curvature, which supports the application of RSM for
513 optimization. Higher adsorbent dosages and lower Cu²⁺ concentrations yield the best results,
514 making them the most important variables to regulate during scale-up or field applications.
515 Figure 11 presents the correlation between actual and predicted values of Cu²⁺ removal using the
516 WsBio-LDH composite adsorbent, while RSM optimized conditions for Cu²⁺ removal using the
517 WsBio-LDH composite adsorbent is shown in Figure 12.



518

519 **Figure 11.** Correlation between actual and predicted values of Cu^{2+} removal using the WsBio-
520 LDH composite adsorbent.



521
522 **Figure 12.** RSM optimized conditions for Cu^{2+} removal using the WsBio-LDH composite
523 adsorbent.

524 Through RSM technique, the adsorption efficiency of copper ions using the WsBio-LDH
525 composite was thoroughly assessed. The effects of four independent variables, contact time,
526 adsorbent dosage, pH, and initial Cu^{2+} concentration on the adsorption performance were
527 investigated using the BBD. The robustness of the RSM model was validated by the
528 experimental data (Table 4), which showed strong consistency with anticipated values. Under
529 optimal conditions, the percentage error was minimum at 0.10 percent. At optimal conditions
530 (87.06 min contact time, 0.491 g WsBio-LDH composite dosage, pH 5.93, and initial Cu^{2+}
531 concentration of 12.75 mg/L), the greatest Cu^{2+} removal efficiency recorded was 99.51% (Table
532 4). The synergistic interaction between LDH and the WS biochar matrix, which offers a large

533 number of active sites and enhanced surface charge properties at a pH close to neutral, favoring
 534 electrostatic interactions with Cu²⁺ ions, is responsible for this high removal efficiency.

535 **Table 4.** Design of experiments and experimental and predicted values for the adsorption
 536 efficiency of the WsBio-LDH composite adsorbent against Cu²⁺.

Run	t (min)	Adsorbent		Cu ²⁺		
		Dose (g)	pH	Conc. (mg/L)	Actual Cu ²⁺ removal (%)	Predicted Cu ²⁺ removal (%)
1	60.5	0.275	4	40	80.00	79.85
2	1	0.05	2	70	38.91	40.54
3	60.5	0.275	4	40	80.00	79.85
4	120	0.5	2	10	81.71	83.88
5	1	0.5	2	70	54.59	56.14
6	60.5	0.275	4	40	80.00	79.85
7	60.5	0.5	4	40	85.02	85.5
8	120	0.05	2	70	54.70	53.73
9	60.5	0.275	6	40	88.12	89.18
10	1	0.05	6	10	61.86	65.2
11	1	0.05	2	10	50.24	47.89
12	120	0.05	6	70	72.50	74.13
13	60.5	0.275	4	40	80.00	79.85
14	60.5	0.275	4	40	80.00	79.85
15	120	0.5	2	70	70.38	67.78
16	1	0.5	2	10	65.92	65.03
17	1	0.5	6	70	83.72	82.2
18	60.5	0.05	4	40	69.34	69.14
19	120	0.05	2	10	66.03	68.29
20	60.5	0.275	4	40	80.00	79.85
21	1	0.5	6	10	83.72	83.89
22	60.5	0.275	4	70	74.85	76.6

23	120	0.275	4	40	80.19	79.42
24	120	0.05	6	10	83.83	81.48
25	60.5	0.275	2	40	70.32	69.55
26	120	0.5	6	70	88.18	89.73
27	1	0.05	6	70	68.04	65.06
28	120	0.5	6	10	99.51	98.62
29	60.5	0.275	4	10	86.18	84.72
30	1	0.275	4	40	64.40	65.46

537 Analysis of variance (ANOVA) revealed that the quadratic model was extremely significant ($p <$
538 0.0001) (Table 5). Outstanding model fit and predictability exhibited by its high R^2 value of
539 0.9854 , adjusted R^2 of 0.9719 , and predicted R^2 of 0.8839 . The four main effects of the
540 independent variables, contact time (A), pH (C), WsBio-LDH composite dose (B), and Cu^{2+}
541 concentration (D), were all statistically significant ($p < 0.0001$), which means that they all
542 affected the adsorption efficiency WsBio-LDH composite for Cu^{2+} . According to the regression
543 model, pH had the biggest positive coefficient (+9.81), followed by adsorbent dose (+8.18) and
544 contact time (+6.98), whereas initial Cu^{2+} concentration had a negative effect (-4.06). These
545 findings imply that while larger initial metal ion concentrations may reduce removal
546 effectiveness due to the saturation of accessible active sites, increasing the pH and dosage
547 significantly improves adsorption.

548 **Table 5.** Analysis of variance (ANOVA) for Cu^{2+} adsorption efficiency of WsBio-LDH
549 composite adsorbent.

Model	Quadratic	Significance
Intercept	79.85	
Model P Value	< 0.0001	Significant
A-t	< 0.0001	Significant
B-LDH/W.B. Dose	< 0.0001	Significant
C-pH	< 0.0001	Significant
D-Cu Conc.	< 0.0001	Significant
AB	0.4903	Not significant
AC	0.079	Not significant

AD	0.0049	Significant
BC	0.4903	Not significant
BD	0.4903	Not significant
CD	0.0049	Significant
A ²	< 0.0001	Significant
B ²	0.0818	Not significant
C ²	0.7236	Not significant
D ²	0.5609	Not significant
Lack of Fit	0.6253	Not significant
R ²	0.9854	
Adjusted R ²	0.9719	
Predicted R ²	0.8839	

550

551 The combined influence of these variable pairs appears to have a significant impact on Cu²⁺
552 uptake, as evidenced by the statistical significance ($p < 0.05$) of interaction terms like AD
553 (contact time and Cu²⁺ concentration) and CD (pH and Cu²⁺ concentration). Notably, a favorable
554 pH at lower concentrations provided ideal binding conditions, whereas a larger Cu²⁺
555 concentration combined with a shorter contact period decreased removal efficacy.

556 Remarkably, the model's accuracy and sufficiency in forecasting the reaction are validated by the
557 non-significant lack of fit ($p = 0.6253$). These results are further supported by the 3D surface and
558 contour plots (Figure not shown here), which graphically depict the interactions and effects of
559 the factors under study. Finally, the predicted and observed response values of WsBio-LDH
560 composite for Cu²⁺ under optimized conditions are shown in Table 6 while the model equation
561 can be written as follows;

$$562 \text{ \% Cu removal} = +79.85 + 6.98A + 8.18B + 9.81C - 4.06D - 0.3864AB - 1.03AC - 1.8AD + 0.3864BC -$$

$$563 0.3864BD + 1.8CD - 7.41A^2 - 2.53B^2 - 0.4892C^2 + 0.8074D^2$$

564

565

566 **Table 6:** Predicted and observed response values of WsBio-LDH composite for Cu²⁺ under
 567 optimized conditions.

Number	t (min)	Adsorbent Dose (g)	pH	Cu ²⁺ Conc. (mg/L)	Cu ²⁺ Removal (%)	Desirability
1	87.058	0.491	5.927	12.754	Predicted 99.61	1
					Actual 99.51	
					% error 0.10	

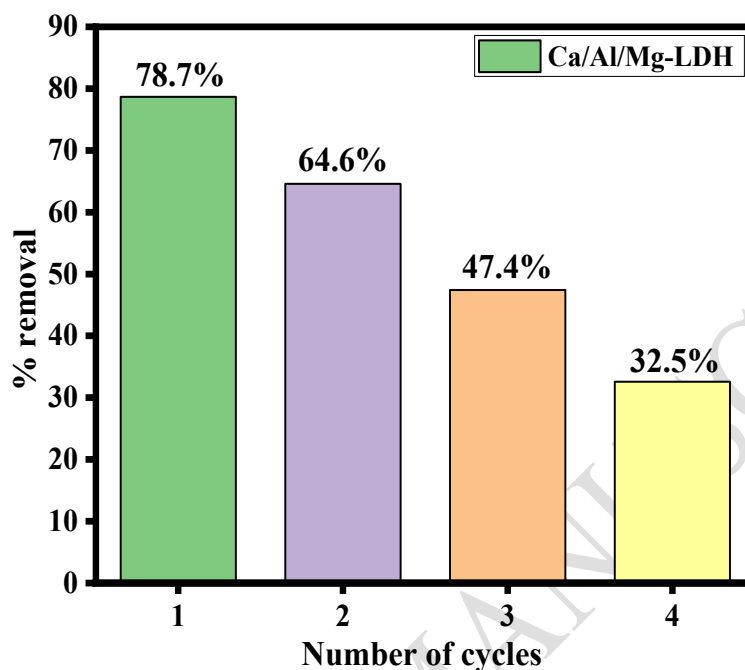
568 This work demonstrates the remarkable adsorption ability of the WsBio-LDH composite under
 569 ideal circumstances, indicating its potential for effective removal of Cu²⁺ from aqueous
 570 solutions. A promising approach to creating affordable, environmentally friendly, and highly
 571 effective adsorbents for heavy metal cleanup is the incorporation of LDH into charcoal matrices.

572 *Recyclability performance of the WsBio-LDH composite*

573 The reusability performance of the WsBio-LDH composite over multiple adsorption desorption
 574 cycles is illustrated in Figure 13. Reusability and stability of the WsBio-LDH composite are
 575 critical for practical applications, particularly in wastewater treatment. To evaluate these
 576 properties, sorption desorption cycles were conducted over four consecutive experiments. For
 577 desorption, 0.1 M HCl was used as the desorption reagent, and agitate it for three hours after
 578 adsorption. The results demonstrated the composite exhibited high initial efficiency, with a Cu²⁺
 579 removal rate of 78.7% in the first cycle. However, in the subsequent three cycles, the removal
 580 efficiency gradually decreased to 64.6%, 47.4%, and 32.5%, respectively, as shown in Figure 13.
 581 This decrease in adsorption efficiency over the cycles may be attributed to the formation of
 582 strong chemical interactions among Cu²⁺ ions and the WsBio-LDH composite, which could
 583 restrict the regeneration of active sites on the WsBio-LDH composite (Shafiq et al. 2025).
 584 Despite the slight decrease, the WsBio-LDH composite maintained a high adsorption efficiency
 585 of 32.5% after four cycles, demonstrating good stability and reusability, making it a promising
 586 candidate for wastewater treatment applications.

587 The adsorption efficiency decreased progressively from 78.7% during the first cycle to 32.5% after the
 588 fourth regeneration cycle. This reduction may be attributed to partial blockage of active adsorption sites,
 589 structural alterations of the LDH layers, and incomplete desorption of previously adsorbed Cu²⁺ ions.
 590 Although the adsorption capacity declined after repeated use, the composite retained measurable removal

591 capability throughout the regeneration cycles. These findings indicate that further improvements in
 592 regeneration procedures and structural stabilization strategies are required to enhance long-term
 593 reusability.



594
 595 **Figure 13.** Reusability studies of Cu²⁺ adsorption onto the WsBio-LDH composite (Cu²⁺ conc. =
 596 30 ppm, dose = 0.3 g, rpm = 220, pH = 6, time = 1 h).

597 **Comparison of Adsorbents**

598 A comparative evaluation of Cu²⁺ adsorption capacity of the WsBio-LDH composite with other
 599 reported adsorbents is presented in Table 7. The WsBio-LDH composite is compared with the
 600 other natural biochar for copper removal (Table 7), which showed good adsorption capacity for
 601 Cu²⁺ under optimal conditions, due to its functionalized surface, and displayed effective
 602 interaction with copper (II) ions in solution.

603 **Table 7.** Comparison of adsorption capacities of different adsorbents for removal of copper ions.

Adsorbent	Concentration range of Cu ²⁺ (mg/L)	Contact time (min)	Sorbent dosage (g)	Adsorption capacity (mg/g)	References
WsBio-LDH	70	60	0.4	101.5	Present study

composite					
Magnetic biochar	50	360	1.0	65.55	(Kołodzyńska and Bąk 2018)
sawdust biochar	50	180	1.0	91.74	(Eleryan et al. 2024)
Biochar (solid waste)	100	180	0.1	5	(Hoslett et al. 2019)
Oxidized biochar (chitosan and PEI)	100	1400	4	26.7	(Liu et al. 2021)

604 **Conclusion**

605 This study highlights the potential of the WsBio-LDH composite as a cost-effective and efficient
606 adsorbent for copper ion removal from aqueous solutions. LDH modification of WS biochar
607 enhance its physicochemical characteristics and metal removal efficiency to 99.6% (adsorbent
608 dose of 0.4 g and pH 6.0), which were optimized to 98.6%, respectively, using RSM. Isotherm
609 studies showed that the WsBio-LDH composite followed the Langmuir model, suggesting an
610 enhanced monolayer adsorption capacity. Kinetic analysis confirmed that the PSO model
611 provided the best fit for the adsorbent, indicating that a monolayer adsorption occurred by
612 chemisorption. Characterization of the WsBio-LDH composite using SEM, EDX, and FTIR
613 confirmed its suitability for adsorption applications. SEM analysis revealed a highly porous
614 surface morphology, while FTIR analysis identified key functional groups.

615 The study also examined the effects of contact time, adsorbent dose, pH, and metal ion
616 concentration. Maximum removal efficiency of Cu^{2+} ions was observed at lower Cu^{2+}
617 concentration, higher pH 6, and optimum adsorbent dose 0.4 g. RSM verified a good connection
618 between statistical and experimental values with an error range of less than 1%. These findings
619 suggest that the WsBio-LDH composite is an effective, cost-efficient, and sustainable adsorbent
620 for the remediation of heavy metals from wastewater. Compared with previously reported
621 biochar-based adsorbents, the WsBio-LDH composite demonstrates superior Cu^{2+} removal
622 efficiency (>99.5%) under optimized conditions, outperforming wheat straw biochar and several
623 metal-oxide-modified biochars reported in the literature. The enhanced performance is attributed

624 to the synergistic effect of LDH incorporation, which increases surface charge density, active
625 binding sites, and ion-exchange capacity.

626 A limitation of the present study is the gradual decline in adsorption efficiency during repeated
627 regeneration cycles. The removal efficiency decreased from 78.7% to 32.5% after four cycles,
628 indicating the need for improved regeneration methods and enhanced structural stability of the
629 composite. Future studies should focus on optimizing regeneration protocols and evaluating
630 long-term performance under continuous treatment conditions.

631 Despite the promising adsorption performance, certain limitations should be acknowledged. The
632 adsorption experiments were conducted under batch conditions using synthetic wastewater,
633 which may not fully represent complex industrial effluents comprising competing ions.
634 Additionally, regeneration efficiency decreased after multiple cycles, indicating partial loss of
635 active adsorption sites. These limitations highlight the need for further investigation under
636 continuous-flow systems and real wastewater conditions.

637 **Future Scope and Practical Applications**

638 The proposed WsBio-LDH composite shows strong potential for real-time wastewater treatment
639 applications due to its low-cost raw material, simple synthesis route, and high adsorption
640 efficiency. Future research may focus on scaling up the process using fixed-bed or continuous-
641 flow reactors, evaluating performance in real industrial effluents, and exploring adsorption of
642 multi-metal systems. Additionally, integration of this adsorbent into hybrid treatment systems
643 could enhance overall removal efficiency and sustainability.

644

645 ***Competing interests***

646 The authors have no relevant financial or non-financial interests to disclose.

647

648 ***Funding***

649 This research work was financially supported by the Vice Deanship of Research Chairs, King
650 Saud University, Riyadh, KSA.

651

652

653

654 **Data Availability Statement**

655 The datasets generated and analyzed during the current study are available from the
656 corresponding author upon reasonable request.

657

658 **References**

659 Abdipour H., and Hemati H. (2024). Sonocatalytic process of penicillin removal using - Fe₂O₃ / effect of
660 different parameters / degradation mechanism/ kinetic study/optimisation with response surface
661 model. *International Journal of Environmental Analytical Chemistry*, 104(20), 8617–8638.
662 <https://doi.org/10.1080/03067319.2023.2207465>

663 Adachi-Pagano M., Forano C., and Besse J.-P. (2003). Synthesis of Al-rich hydrotalcite-like compounds
664 by using the urea hydrolysis reaction—control of size and morphology. *Journal of Materials*
665 *Chemistry*, 13(8), 1988–1993. <https://doi.org/10.1039/B302747N>

666 Afshar M., and Mofatteh S. (2024). Biochar for a sustainable future: Environmentally friendly production
667 and diverse applications. *Results in Engineering*, 23, 102433.
668 <https://doi.org/10.1016/j.rineng.2024.102433>

669 Akhtar M., Sarfraz M., Ahmad M., Raza N., and Zhang L. (2025). Use of low-cost adsorbent for waste
670 water treatment: Recent progress, new trend and future perspectives. *Desalination and Water*
671 *Treatment*, 321, 100914. <https://doi.org/10.1016/j.dwt.2024.100914>

672 Alprol A. E., Mansour A. T., Ibrahim M. E. E.-D., Ashour M., Alprol A. E., Mansour A. T., Ibrahim M. E.
673 E.-D., and Ashour M. (2024). Artificial Intelligence Technologies Revolutionizing Wastewater
674 Treatment: Current Trends and Future Prospective. *Water*, 16(2), 314.
675 <https://doi.org/10.3390/w16020314>

676 Al-Rashdi B. A. M., Johnson D. J., and Hilal N. (2013). Removal of heavy metal ions by nanofiltration.
677 *Desalination*, 315, 2–17. <https://doi.org/10.1016/j.desal.2012.05.022>

678 Bayantong A. R. B., Shih Y.-J., Ong D. C., Abarca R. R. M., Dong C.-D., and de Luna M. D. G. (2021).
679 Adsorptive removal of dye in wastewater by metal ferrite-enabled graphene oxide
680 nanocomposites. *Chemosphere*, 274, 129518. <https://doi.org/10.1016/j.chemosphere.2020.129518>

681 Bej S., Swain S., Bishoyi A. K., Mandhata C. P., Sahoo C. R., and Padhy R. N. (2023). Wastewater-
682 Associated Infections: A Public Health Concern. *Water, Air, & Soil Pollution*, 234(7), 444.
683 <https://doi.org/10.1007/s11270-023-06431-4>

684 Biswal B. K., and Balasubramanian R. (2023). Use of biochar as a low-cost adsorbent for removal of
685 heavy metals from water and wastewater: A review. *Journal of Environmental Chemical*
686 *Engineering*, 11(5), 110986. <https://doi.org/10.1016/j.jece.2023.110986>

687 Cao X., Ma L., Gao B., and Harris W. (2009). Dairy-Manure Derived Biochar Effectively Sorbs Lead and
688 Atrazine. *Environmental Science & Technology*, 43(9), 3285–3291.
689 <https://doi.org/10.1021/es803092k>

690 Chen R., Gan C., Cai B., Liu R., Xu W., Yin W., Li H., Yu L., and Yong Q. (2024). Co-adsorption and
691 selective-adsorption of heavy metals and dyes from aqueous solution by bio-based
692 humus/chitosan hydrogels. *Journal of Environmental Sciences*, 145, 193–204.
693 <https://doi.org/10.1016/j.jes.2023.09.004>

694 Cheung W. H., Szeto Y. S., and McKay G. (2007a). Intraparticle diffusion processes during acid dye
695 adsorption onto chitosan. *Bioresource Technology*, 98(15), 2897–2904.
696 <https://doi.org/10.1016/j.biortech.2006.09.045>

697 Cheung W. H., Szeto Y. S., and McKay G. (2007b). Intraparticle diffusion processes during acid dye
698 adsorption onto chitosan. *Bioresource Technology*, 98(15), 2897–2904.
699 <https://doi.org/10.1016/j.biortech.2006.09.045>

700 Das S., Singh C. K., Sodhi K. K., and Singh V. K. (2025). Circular economy approaches for water reuse
701 and emerging contaminant mitigation: innovations in water treatment. *Environment, Development*
702 *and Sustainability: A Multidisciplinary Approach to the Theory and Practice of Sustainable*
703 *Development*, 27(3), 5753–5794. <https://doi.org/10.1007/s10668-023-04183-z>

704 Dehghani M. H., Ahmadi S., Ghosh S., Othmani A., Osagie C., Meskini M., AlKafaas S. S., Malloum A.,
705 Khanday W. A., Jacob A. O., Gökkuş Ö., Oroke A., Martins Chineme O., Karri R. R., and Lima
706 E. C. (2023). Recent advances on sustainable adsorbents for the remediation of noxious pollutants
707 from water and wastewater: A critical review. *Arabian Journal of Chemistry*, 16(12), 105303.
708 <https://doi.org/10.1016/j.arabjc.2023.105303>

709 Elbagory M., EL-Khateeb N., El-Nahrawy S., El-Dein Omara A., Mohamed I., El-Sharkawy M., Zayed
710 A., Goala M., Gupta D., Kumar P., Kumar P., and Širić I. (2025). Inclusion of key soil parameters
711 in the modified contamination factor (MCF) model as a tool for assessing heavy metal pollution
712 in agricultural soils. *Scientific Reports*, 15(1), 42974. [https://doi.org/10.1038/s41598-025-27110-](https://doi.org/10.1038/s41598-025-27110-w)
713 [w](https://doi.org/10.1038/s41598-025-27110-w)

714 Eleryan A., Aigbe U. O., Ukhurebor K. E., Onyancha R. B., Eldeeb T. M., El-Nemr M. A., Hassaan M. A.,
715 Ragab S., Osibote O. A., Kusuma H. S., Darmokoesoemo H., and El Nemr A. (2024). Copper(II)
716 ion removal by chemically and physically modified sawdust biochar. *Biomass Conversion and*
717 *Biorefinery*, 14(8), 9283–9320. <https://doi.org/10.1007/s13399-022-02918-y>

718 El-Shafey S. E., Obada M. K., El-Shamy A. M., and Mohamed W. S. (2024). Silica/kluclen nanocomposite
719 as promising durable adsorbent for lead removal from industrial effluents. *Scientific Reports*,
720 14(1), 26095. <https://doi.org/10.1038/s41598-024-74680-2>

721 Farooq, A., Li, X., Pan, G., Liu, Q., Wang, F., Chen, S., Zhao, G. and Hussain, F., (2025). Advancing
722 green textile modification with deep eutectic solvents: from solvent design to industrial prospects.
723 *Journal of Molecular Liquids*, 347(B), 128501. <https://doi.org/10.1016/j.molliq.2025.128501>.

724 Fouad, E.A., Ahmad, F. and Ahmed, N. (2017). Optimization of chromium extraction from aqueous
725 solutions by emulsion liquid membrane. *Desalination and Water Treatment*, 65, 428-434.
726 <https://doi.org/10.5004/dwt.2017.20287> Frost R. L., and Kloprogge J. T. (1999). Infrared
727 emission spectroscopic study of brucite. *Spectrochimica Acta Part A: Molecular and*
728 *Biomolecular Spectroscopy*, 55(11), 2195–2205. [https://doi.org/10.1016/S1386-1425\(99\)00016-5](https://doi.org/10.1016/S1386-1425(99)00016-5)

729 Gaetke L. M., Chow-Johnson H. S., and Chow C. K. (2014). Copper: toxicological relevance and
730 mechanisms. *Archives of Toxicology*, 88(11), 1929–1938. [https://doi.org/10.1007/s00204-014-](https://doi.org/10.1007/s00204-014-1355-y)
731 [1355-y](https://doi.org/10.1007/s00204-014-1355-y)

732 Gräf T., Gummi K., Filser J., Thöming J., and Köser J. (2023). Improving Membrane Filtration for
733 Copper Speciation: Optimal Salt Pretreatments of Polyethersulfone Membranes to Prevent
734 Analyte Retention. *ACS Omega*, 8(6), 5742–5751. <https://doi.org/10.1021/acsomega.2c07355>

735 Hagag M. A., El-Gayar D. A., Nosier S. A., and Mubarak A. A. (2017). Removal of heavy metals from
736 industrial waste solutions by a rotating fixed bed of ion exchange resin. *Desalination and Water
737 Treatment*, 100, 178–184. <https://doi.org/10.5004/dwt.2017.21794>

738 Haleem N., Khattak A., Jamal Y., Sajid M., Shahzad Z., and Raza H. (2022). Development of poly vinyl
739 alcohol (PVA) based biochar nanofibers for carbon dioxide (CO₂) adsorption. *Renewable and
740 Sustainable Energy Reviews*, 157, 112019. <https://doi.org/10.1016/j.rser.2021.112019>

741 Han F., Hessen A. S., Amari A., Elboughdiri N., and Zahmatkesh S. (2024). Heavy metal (Cu²⁺) removal
742 from wastewater by metal-organic framework composite adsorbent: Simulation-based- artificial
743 neural network and response surface methodology. *Environmental Research*, 245, 117972.
744 <https://doi.org/10.1016/j.envres.2023.117972>

745 Hassan, A. M. M., Asif, M., Al-Mansur, M. A., Uddin, M. R., Alsufyani, S. J., Yasmin, F., & Khandaker,
746 M. U. (2023). Characterization of municipal solid waste for effective utilization as an alternative
747 source for clean energy production. *Journal of Radiation Research and Applied Sciences*, 16(4),
748 100683. <https://doi.org/10.1016/j.jrras.2023.100683>.

749 Hoslett J., Ghazal H., Ahmad D., and Jouhara H. (2019). Removal of copper ions from aqueous solution
750 using low temperature biochar derived from the pyrolysis of municipal solid waste. *Science of
751 The Total Environment*, 673, 777–789. <https://doi.org/10.1016/j.scitotenv.2019.04.085>

752 Hussain, M. S., Ahmed, S., Irshad, M., Bibi, S. S., Asif, M., Sher, F., & Khan, M. K. (2024). Recent
753 engineering strategies for enhancing C₂⁺ product formation in copper-catalyzed CO₂

754 electroreduction. *Nano Materials Science*, 8(1), 207-233.
755 <https://doi.org/10.1016/j.nanoms.2024.09.001>.

756 Hussain N., Asif M., Shafaat S., Khan M. S., Riaz N., Iqbal M., Javed A., Butt T. A., Shaikh A. J., and
757 Bilal M. (2025). Multilayer adsorption of reactive orange 16 dye onto Fe₂O₃/ZnO hybrid
758 nanoadsorbent: mechanistic insights from kinetics, isotherms and dynamic light scattering
759 studies. *Journal of Chemical Technology & Biotechnology*, 100(1), 50–66.
760 <https://doi.org/10.1002/jctb.7753>

761 Johnston A.-L., Lester E., Williams O., and Gomes R. L. (2021). Understanding Layered Double
762 Hydroxide properties as sorbent materials for removing organic pollutants from environmental
763 waters. *Journal of Environmental Chemical Engineering*, 9(4), 105197.
764 <https://doi.org/10.1016/j.jece.2021.105197>

765 Jafari A. J., Mansoorian H. J., Askarpour H., Salari M., Eslami F., Faraji M., Shomoossi F., Abdipour H.,
766 and Ansari F. J. (2025). Analyzing and optimizing the adsorption of metronidazole antibiotic on
767 nano-scale pumice mine waste based RSM-CCD technique in water. *International Journal of*
768 *Environmental Science and Technology*, 22(6), 4091–4108. [https://doi.org/10.1007/s13762-024-](https://doi.org/10.1007/s13762-024-06102-9)
769 [06102-9](https://doi.org/10.1007/s13762-024-06102-9)

770 Kabir E., Kim K.-H., and Kwon E. E. (2023). Biochar as a tool for the improvement of soil and
771 environment. *Frontiers in Environmental Science*, 11.
772 <https://doi.org/10.3389/fenvs.2023.1324533>

773 Kameliya J., Verma A., Dutta P., Arora C., Vyas S., and Varma R. S. (2023). Layered Double Hydroxide
774 Materials: A Review on Their Preparation, Characterization, and Applications. *Inorganics*, 11(3),
775 Article 3. <https://doi.org/10.3390/inorganics11030121>

776 Kołodzyńska D., and and Bąk J. (2018). Use of three types of magnetic biochar in the removal of
777 copper(II) ions from wastewaters. *Separation Science and Technology*, 53(7), 1045–1057.
778 <https://doi.org/10.1080/01496395.2017.1345944>

779 Kouniba S., Benbiyi A., Zourif A., and EL Guendouzi M. (2024). Optimization use of watermelon rind in
780 the coagulation-flocculation process by Box Behnken design for copper, zinc, and turbidity
781 removal. *Heliyon*, 10(10), e30823. <https://doi.org/10.1016/j.heliyon.2024.e30823>

782 Kumar A., Schreiter I. J., Wefer-Roehl A., Tsechansky L., Schüth C., and Graber E. R. (2016). Chapter 5 -
783 Production and Utilization of Biochar From Organic Wastes for Pollutant Control on
784 Contaminated Sites. In M. N. V. Prasad & K. Shih (Eds.), *Environmental Materials and Waste*
785 (pp. 91–116). Academic Press. <https://doi.org/10.1016/B978-0-12-803837-6.00005-6>

786 Liang, S., Feng, X., Li, X., Wang, Z., Miao, K., Feng, G. and Luo, X., 2026 Catalysis of
787 nonstoichiometric Mn–Co spinel oxides in effective peroxymonosulfate activation: Structure–
788 activity relationship and flow-through organic wastewater treatment. *Separation and Purification*
789 *Technology*, 397(3), 138142. <https://doi.org/10.1016/j.seppur.2026.138142>.

790 Liu J., and Wang X. (2013a). Novel Silica-Based Hybrid Adsorbents: Lead(II) Adsorption Isotherms. *The*
791 *Scientific World Journal*, 2013(1), 897159. <https://doi.org/10.1155/2013/897159>

792 Liu J., and Wang X. (2013b). Novel Silica-Based Hybrid Adsorbents: Lead(II) Adsorption Isotherms. *The*
793 *Scientific World Journal*, 2013(1), 897159. <https://doi.org/10.1155/2013/897159>

794 Liu Q., Zang G.-L., and Zhao Q. (2021). Removal of copper ions by functionalized biochar based on a
795 multicomponent Ugi reaction. *RSC Advances*, 11(42), 25880–25891.
796 <https://doi.org/10.1039/D1RA04156H>

797 Li, X., Li, Y., Li, Y., Zhang, M., & Zhu, J. (2026). Synthesis of Lignin-Derived Hierarchical Porous
798 Carbon via Hydrothermal–Phosphoric Acid Synergistic Activation for Enhanced Adsorption of
799 Tetracycline. *Molecules*, 31(3), 447, <https://doi.org/10.3390/molecules31030447>

800 Li, X., Ran, R., Zeng, W., Ren, S., Wang, Y., Zhu, A., & Zheng, C. (2025). Coffee shell as a green
801 reductant for iron recovery from pyrite cinder: synergy of biomass-driven reduction and acid
802 leaching. *Minerals Engineering*, 234, 109747, <https://doi.org/10.1016/j.mineng.2025.109747>.

803

804 Liu Y., Gao C., Liu L., Li Y., and Guo X. (2025). A photovoltaic powered ocean-based electrochemical
805 system produces highly oxidizing active substances for simultaneous removal of antibiotics and
806 heavy metals from mariculture wastewater. *Water Research*, 286, 124177.
807 <https://doi.org/10.1016/j.watres.2025.124177>

808 Luo Y., Gao B., Yue Q., and Li R. (2018). Application of enteromorpha polysaccharides as coagulant aid
809 in the simultaneous removal of CuO nanoparticles and Cu²⁺: Effect of humic acid concentration.
810 *Chemosphere*, 204, 492–500. <https://doi.org/10.1016/j.chemosphere.2018.03.168>

811 Lyu P., Li L., Huang J., Ye J., Zhu C., Xie J., Wang Z., Kang M., and Yan A. (2023). Enhancing sorption
812 of layered double hydroxide-based magnetic biochar for arsenic and cadmium through optimized
813 preparation protocols. *Bioresource Technology*, 388, 129756.
814 <https://doi.org/10.1016/j.biortech.2023.129756>

815 Ma Q., Qian Y., Su W., Shi L., Wang E., Yu A., Zheng J., and Lu Y. (2025). Degradation of agricultural
816 polyethylene film by greater wax moth (*Galleria mellonella*) larvae and screening of involved gut
817 bacteria. *Ecotoxicology and Environmental Safety*, 303, 118841.
818 <https://doi.org/10.1016/j.ecoenv.2025.118841>

819 Mahmood, Z., Abbas, N., Naqvi, S.A.R., Gilani, M.R.H.S., Hussain, F., Ali, S.K., Iqbal, S., Mahmood, S.,
820 Abdelmohsen, S.A. and Alarfj, S.F. (2026). Visible-Light-Activated CuFe₂O₄/Zn-BTC
821 Photocatalyst for Efficient Mineralization and Detoxification of Carbofuran in Industrial
822 Effluents. *Catalysis Letters*, 156(6), 176. <https://doi.org/10.1007/s10562-026-05418-0>.

823 Mingming S., Hengze Z., Ye L., and Lingqi Z. (2023). The adsorption properties of steel slag-based
824 porous geopolymers for Cu²⁺ removal. *Minerals Engineering*, 201, 108225.
825 <https://doi.org/10.1016/j.mineng.2023.108225>

826 Mokhtar M., Dickson S. E., Kim Y., and Mekky W. (2018). Preparation and characterization of ion
827 selective membrane and its application for Cu²⁺ removal. *Journal of Industrial and Engineering*
828 *Chemistry*, 60, 475–484. <https://doi.org/10.1016/j.jiec.2017.11.035>

829 Mondal M. K. (2009). Removal of Pb(II) ions from aqueous solution using activated tea waste:
830 Adsorption on a fixed-bed column. *Journal of Environmental Management*, 90(11), 3266–3271.
831 <https://doi.org/10.1016/j.jenvman.2009.05.025>

832 Nzediegwu C., Naeth M. A., and Chang S. X. (2021). Elemental composition of biochars is affected by
833 methods used for its determination. *Journal of Analytical and Applied Pyrolysis*, 156, 105174.
834 <https://doi.org/10.1016/j.jaap.2021.105174>

835 Othman C. S., Salih Y. M., and Hamasalih L. O. (2023). Adsorption desulfurization of dibenzothiophene
836 in a model and diesel fuel by hybrid activated charcoal/mixed metal oxide. *Petroleum Science
837 and Technology*, 41(22), 2121–2140. <https://doi.org/10.1080/10916466.2022.2108052>

838 Patel M. R., and Panwar N. L. (2023). Biochar from agricultural crop residues: Environmental,
839 production, and life cycle assessment overview. *Resources, Conservation & Recycling Advances*,
840 19, 200173. <https://doi.org/10.1016/j.rcradv.2023.200173>

841 Priya K., Rani J., and Gwal S. (2025). Chapter 6 - Transforming agricultural residues to value-added
842 products: waste to wealth. In S. Rai, A. K. Bhardwaj, & L. M. Colla (Eds.), *Sustainable
843 Management of Agro-Food Waste* (pp. 69–85). Academic Press. <https://doi.org/10.1016/B978-0-443-23679-2.00006-9>

844

845 Qin, X., Cui, H., & Zhou, Q. (2023). Physisorption behaviors of organochlorine pesticides on the InP3
846 monolayer from theoretical insight. *ACS omega*, 8(35), 32168-32175,
847 <https://doi.org/10.1021/acsomega.3c04665>.

848 Rashid R., Shafiq I., Akhter P., Iqbal M. J., and Hussain M. (2021). A state-of-the-art review on
849 wastewater treatment techniques: the effectiveness of adsorption method. *Environmental Science
850 and Pollution Research*, 28(8), 9050–9066. <https://doi.org/10.1007/s11356-021-12395-x>

851 Rishch R. S., Vazvani M. G., Hassanisaadi M., and Thakur V. K. (2024). Agricultural wastes: A practical
852 and potential source for the isolation and preparation of cellulose and application in agriculture
853 and different industries. *Industrial Crops and Products*, 208, 117904.
854 <https://doi.org/10.1016/j.indcrop.2023.117904>

855 Rydz J., Šišková A., and Andicsová Eckstein A. (2019). Scanning Electron Microscopy and Atomic Force
856 Microscopy: Topographic and Dynamical Surface Studies of Blends, Composites, and Hybrid
857 Functional Materials for Sustainable Future. *Advances in Materials Science and Engineering*,
858 2019(1), 6871785. <https://doi.org/10.1155/2019/6871785>

859 Olugbenga S. O., Adeleye P. G, Oladipupo S. B, Adeleye A. T, and John K. I. (2024). Biomass-derived
860 biochar in wastewater treatment- a circular economy approach. *Waste Management Bulletin*, 1(4),
861 1–14. <https://doi.org/10.1016/j.wmb.2023.07.007>

862 Shafiq M., Alazba A. A., and Amin M. T. (2025). Eco-friendly nanocomposite of manganese-iron and
863 plant waste derived biochar for optimizing Pb²⁺ adsorption: A response surface methodology
864 approach. *Desalination and Water Treatment*, 322, 101091.
865 <https://doi.org/10.1016/j.dwt.2025.101091>

866 Shiriazar M. A., Sepehr E., Maleki R., Khodaverdiloo H., Asadzadeh F., Dovlati B., and Rengel Z.
867 (2022). Arsenate removal from aqueous solutions by Mg/Fe-LDH-modified biochar derived from
868 apple tree residues. *Earth and Environmental Science Transactions of The Royal Society of*
869 *Edinburgh*, 113(2), 149–158. <https://doi.org/10.1017/S1755691022000019>

870 Shoudho K. N., Khan T. H., Ara U. R., Khan M. R., Shawon Z. B. Z., and Hoque M. E. (2024). Biochar in
871 global carbon cycle: Towards sustainable development goals. *Current Research in Green and*
872 *Sustainable Chemistry*, 8, 100409. <https://doi.org/10.1016/j.crgsc.2024.100409>

873 Sun X., Li S., Xiong Y., and You Y. (2022). Flocculation performance and evaluation of a sulfur-
874 containing tannin flocculant for Cu²⁺ removal. *Separation and Purification Technology*, 303,
875 122277. <https://doi.org/10.1016/j.seppur.2022.122277>

876 Syed, N.H., Haq, I., Ahmad, F., Khan, N.A., Habib, M., Ahmad, N. and Rind, I.K., (2024). A Low Cost
877 Wastewater Reclamation Unit comprising a Lamella Settler for reducing Fresh Water Usage in
878 Carwash Stations. *Engineering, Technology & Applied Science Research*, 14(5), 16221-16228.
879 <https://doi.org/10.48084/etasr.8066>.

880 Tabassam M. N., Haseeb M., Habib M. A. B., Murtaza R., Ali S., Malik M. R., Numan M., Mahmood M.,
881 Mustafa Z., and Khan W. Z. (2025). Next-Generation Adsorbents for Wastewater Remediation: A
882 Nanotechnology-Driven and AI-Enabled Breakthrough Towards Clean Water. *Scholars Journal of*
883 *Physics, Mathematics and Statistics*, 12(08), 323–345.
884 <https://doi.org/10.36347/sjpms.2025.v12i08.001>

885 Tanweer, A., Taqvi, S. A. A., Kazmi, B., Khatoun, S., Taha, M., Nadir, M., . . . Ahmad, N. (2025).
886 Advancing algae-based Bioenergy: Techno-Economic assessment of hydrogen and biochar
887 production from algal biomass. *Biomass and Bioenergy*, 200, 108039,
888 <https://doi.org/10.1016/j.biombioe.2025.108039>

889 Torabideh M., Khalooei M., Rajabizadeh A., Abdipour H., and Zeinali S. (2025). Optimisation of mercury
890 adsorption by ZIF-8 from aqueous solutions through response surface methodology. *International*
891 *Journal of Environmental Analytical Chemistry*, 105(18), 6910–6932.
892 <https://doi.org/10.1080/03067319.2024.2432583>

893 Trinh H. B., Lee J., Kim S., Lee J., Aceituno J. C. F., and Oh S. (2021). Selective Recovery of Copper
894 from Industrial Sludge by Integrated Sulfuric Leaching and Electrodeposition. *Metals*, 11(1),
895 Article 1. <https://doi.org/10.3390/met11010022>

896 Wang, D., Hu, W., Zheng, Y., Cheng, H., Lu, X., He, Z., Giannakis, S., Song, S. and Ma, J., (2026).
897 Mechanistic insights into hexamethylphosphoramide degradation and phosphorus recovery via
898 mZVI/O₃: Beyond conventional oxidation through iron-phosphorus speciation. *Chemical*
899 *Engineering Journal*, 538, 176658. <https://doi.org/10.1016/j.cej.2026.176658>.

900 Wang L., Shi C., Wang L., Pan L., Zhang X., and Zou J.-J. (2020). Rational design, synthesis, adsorption
901 principles and applications of metal oxide adsorbents: a review. *Nanoscale*, 12(8), 4790–4815.
902 <https://doi.org/10.1039/C9NR09274A>

903 Wang T., Liu W., Xiong L., Xu N., and Ni J. (2013). Influence of pH, ionic strength and humic acid on
904 competitive adsorption of Pb(II), Cd(II) and Cr(III) onto titanate nanotubes. *Chemical*
905 *Engineering Journal*, 215–216, 366–374. <https://doi.org/10.1016/j.cej.2012.11.029>

- 906 Wang Y., Zheng K., Jiao Z., Zhan W., Ge S., Ning S., Fang S., and Ruan X. (2022). Simultaneous
907 Removal of Cu^{2+} , Cd^{2+} and Pb^{2+} by Modified Wheat Straw Biochar from Aqueous Solution:
908 Preparation, Characterization and Adsorption Mechanism. *Toxics*, 10(6), Article 6.
909 <https://doi.org/10.3390/toxics10060316>
- 910 Xu S., Zhang L., Zhao J., Cheng J., Yu Q., Zhang S., Zhao J., and Qiu X. (2020). Remediation of
911 chromium-contaminated soil using delaminated layered double hydroxides with different divalent
912 metals. *Chemosphere*, 254, 126879. <https://doi.org/10.1016/j.chemosphere.2020.126879>
- 913 Yan F., Chen H., Chi T., Lu J., Shen X., Xie F., Wang P., and Zhang Z. (2025). Highly efficient and
914 regenerable amine-impregnated adsorbents: Mechanistic insights into glycerol modification for
915 enhanced direct air capture. *Chemical Engineering Journal*, 520, 166450.
916 <https://doi.org/10.1016/j.ccej.2025.166450>
- 917 Yrjälä K., and Zheng H. (2021). Renewable Energy from Woody Biomass of Poplar and Willow SRC
918 Coupled to Biochar Production. In P. Pathak & R. Ranjan Srivastava (Eds.), *Alternative Energy*
919 *Resources* (pp. 133–150). Springer. https://doi.org/10.1007/698_2020_647
- 920 Zakaria K. K., Farag H. A., and El-Gayar D. A. (2023). Removal of Cu^{2+} , Fe^{2+} and SO_4^{2-} ions from
921 industrial wastewater by ion exchange resins contained in a rotating perforated cylindrical basket
922 of different heights. *Scientific Reports*, 13(1), 3248. <https://doi.org/10.1038/s41598-023-29956-4>
- 923 Zhang D., Wu B., Wang T., Yılmaz M., Sharma G., Kumar A., and Shi H. (2025). Multi-mechanism
924 synergistic adsorption of lead and cadmium in water by structure-functionally adapted modified
925 biochar: A review. *Desalination and Water Treatment*, 322, 101156.
926 <https://doi.org/10.1016/j.dwt.2025.101156>
- 927 Zhang Y., Luo C., Wang H., Han L., Wang C., Jie X., and Chen Y. (2016). Modified adsorbent
928 hydroxypropyl cellulose xanthate for removal of Cu^{2+} and Ni^{2+} from aqueous solution.
929 *Desalination and Water Treatment*, 57(56), 27419–27431.
930 <https://doi.org/10.1080/19443994.2016.1177733>

931 Zou Y., Liu Y., Wang X., Sheng G., Wang S., Ai Y., Ji Y., Liu Y., Hayat T., and Wang X. (2017). Glycerol-
932 Modified Binary Layered Double Hydroxide Nanocomposites for Uranium Immobilization via
933 Extended X-ray Absorption Fine Structure Technique and Density Functional Theory Calculation.
934 *ACS Sustainable Chemistry & Engineering*, 5(4), 3583–3595.
935 <https://doi.org/10.1021/acssuschemeng.7b00439>

ACCEPTED MANUSCRIPT